UHASSELT
KNOWLEDGE IN ACTION

Maastricht University

Faculty of Medicine and Life Sciences
School for Life Sciences
Master of Biomedical Sciences

Master's thesis

Promoting wound healing and angiogenesis in acute radiation dermatitis: ROS-responsive nanocarriers as an efficient drug delivery system

Hanne Eerdekens

Thesis presented in fulfillment of the requirements for the degree of Master of Biomedical Sciences, specialization Molecular Mechanisms in Health and Disease

SUPERVISOR :

Prof. dr. Annelies BRONCKAERS

MENTOR :

Mevrouw Elke PIRLET

2023
2024

Transnational University Limburg is a unique collaboration of two universities in two countries: the University of Hasselt and Maastricht University.

UHASSELT
KNOWLEDGE IN ACTION

www.uhasselt.be
Universiteit Hasselt
Campus Hasselt:
Martelarenlaan 42 | 3500 Hasselt
Campus Diepenbeek:
Agoralaan Gebouw D | 3590 Diepenbeek

UHASSELT
KNOWLEDGE IN ACTION

Maastricht University

Faculty of Medicine and Life Sciences
School for Life Sciences
Master of Biomedical Sciences

Master's thesis

Promoting wound healing and angiogenesis in acute radiation dermatitis: ROS-responsive nanocarriers as an efficient drug delivery system

Hanne Eerdekens

Thesis presented in fulfillment of the requirements for the degree of Master of Biomedical Sciences, specialization Molecular Mechanisms in Health and Disease

SUPERVISOR :

Prof. dr. Annelies BRONCKAERS

MENTOR :

Mevrouw Elke PIRLET

Enhancing wound healing by promoting angiogenesis in acute radiation dermatitis: ROS-responsive nanocarriers as an efficient drug delivery system.*

Eerdekens H.[1], Pirlet E.[2], and Bronckaers A.[2]

[1]Faculty of Medicine and Life Sciences, Universiteit Hasselt, Campus Diepenbeek, Agoralaan Gebouw D - B-3590 Diepenbeek
[2]Laboratory for research in ischemic stroke, stem cells & angiogenesis (LISSA), Biomedical Research Institute, Universiteit Hasselt, Campus Diepenbeek, Agoralaan Gebouw C - B-3590 Diepenbeek

*Running title: *Nanocarriers as drug delivery system to promote wound healing in radiation dermatitis*.

To whom correspondence should be addressed: Bronckaers A., Tel: +32476582985; Email: annelies.bronckaers@uhasselt.be

Keywords: Radiotherapy, Acute radiation dermatitis, ROS-responsive nanocarriers, Angiogenesis, Inflammation, Wound healing.

ABSTRACT

Radiation therapy (RT) is vital in cancer therapies, but often leads to adverse events, such as acute radiodermatitis (ARD). ARD is characterized by ROS release and vascular damage, resulting in impaired wound healing. With no standardized therapy available, we aim to develop a novel treatment approach using ROS-responsive VEGF-loaded NCs (VEGF NCs) to enhance healing of RT-induced wounds. Initially, we examined if tert-butyl hydroperoxide (tBHP) induces high ROS levels without cytotoxicity. Next, we assessed the uptake, cytotoxicity, and cellular stress of VEGF NCs on HUVEC and the VEGF release of NCs in response to H_2O_2. Finally, we aimed to establish an *in vitro* ARD model through x-ray irradiation and to explore the impact of radiation on VEGF's bioactivity. Our results show that 50 µM tBHP for 3h induced high ROS levels and low cytotoxicity in HUVEC using the FACS, H_2DCFDA, and Alamar Blue assay. Further, qPCR and Ellman reagent assay revealed a tBHP dose-dependent decrease in oxidized glutathione and increased antioxidant gene expression. Moreover, rhodamine B-loaded- and VEGF NCs were biocompatible with HUVEC at low concentrations in the Alamar Blue assay, while efficient NC uptake was observed in FACS and IF staining. Additionally, ELISA results indicated a H_2O_2-induced VEGF release from NCs, enhanced by dextranase. Finally, upon 20 Gy irradiation, HUVECs exhibited elevated ROS levels and preserved cell viability after 24h, whereas 10 Gy reduced VEGF proliferation capacity in HUVEC. To conclude, our findings suggest that VEGF NCs hold significant promise in managing RT-induced wounds.

INTRODUCTION

Radiotherapy (RT) serves as a cornerstone in the treatment of approximately half of all cancer patients globally, numbering in millions annually (1). Despite its effectiveness in treating various cancers, RT also induces a broad range of short-and long-term side effects, including fatigue, skin irritation, nausea, and cognitive impairment (1, 2). Notably, acute radiodermatitis (ARD), characterized by adverse inflammatory skin reactions, stands out as a prevalent concern, affecting over 95% of cancer patients (2-4). ARD typically develops within several days to weeks following RT leading to distressing symptoms. Initially, it manifests as erythema, progressing to dry or wet desquamation with repeated exposure, which can even lead to ulcer formation. Beyond physical discomfort, these symptoms significantly impact the overall quality of life of the patients by

causing pain, discomfort, interfering with daily activities such as bathing, dressing, and sleeping, and affecting self-esteem and emotional well-being due to visible skin changes (2-5). Managing ARD involves a multifaceted approach aimed at alleviating symptoms and supporting skin health. Various skincare routines, administration of corticosteroids, and systemic medications such as antibiotics are utilized to minimize discomfort and promote healing (3, 6, 7).Nevertheless, there is still no uniform consent regarding a robust and scientifically-based therapy, emphasizing the need for a new, evidence-based therapy to enhance wound healing after RT (7-10).

Radiotherapy induces injury through various mechanism, predominantly affecting tissues characterized by rapid cellular division, such as the skin. Consequently, it initiates DNA damage in these cells, causing single or double strand breaks that can result in mutations and ultimately cell death (2, 11-13). Second, the use of high-energy radiation in RT (X-rays or gamma rays), generates reactive oxygen species (ROS) in cells through interactions with water molecules. These ROS include highly reactive molecules like hydroxyl radicals (•OH), superoxide radicals (•O2−), and hydrogen peroxide (H_2O_2), which directly damages various biomolecules in the cell, including nucleic acids, lipids, and proteins (14-16). Moreover, high levels of ROS are also associated with skin inflammation through the stimulation of pro-inflammatory cytokines, such as interleukin (IL)-6, IL-8, and tumor necrosis factor alpha (TNF)-α (17-19). High and prolonged levels of inflammation result in impairment of the skin's ability to heal and regenerate.

Besides damaging the skin, RT also affects endothelial cells (ECs) lining the blood capillaries within the skin, which are crucial for wound healing by transporting oxygen and nutrients to the site of injury (20, 21). Due to the repetitive nature of RT, ROS accumulates inside the skin causing EC death in response to the elevated oxidative stress. Consequently, the delicate blood vessel network is disturbed, leading to blood vessel regression (14). To rebuild the vascular network, the process of angiogenesis is stimulated. This is a crucial physiological mechanism for the formation of new blood vessels, which occurs selectively in response to specific stimuli released into the surrounding environment during injury and inflammation such as the vascular endothelial growth factor (VEGF), fibroblast growth factor (FGF) and angiopoietin (Ang)(22, 23). Recent studies have already underscored the pivotal role of VEGF in promoting angiogenesis both *in vivo* and *in vitro*, highlighting its significance in this process (24-26). Without these angiogenic signals the process of angiogenesis remains inactive, underscoring its dependence on specific molecular cues. Initiation of angiogenesis involves the breakdown of the extracellular matrix surrounding existing blood vessels, facilitating detachment and proliferation of ECs. Subsequently, the presence of angiogenic growth factors attracts ECs, guiding their migration along a chemotactic gradient toward the injury site. Upon arrival, these ECs align into tube-like structures, ultimately leading to the formation of new blood vessels (27-29).

Given the notable impact of RT on blood vessel damage, a promising approach to enhancing wound healing in ARD involves promoting angiogenesis. Although VEGF seems promising for the healing of RT-induced wounds, it has a relatively short *in vivo* half-life, which limits their therapeutic efficacy (30, 31).Consequently, there is a pressing need for efficient drug delivery systems (DDS) to facilitate the sustained local release and actions of VEGF. Various DDS, including liposomes, micelles, and nanoparticles, represent promising approaches for achieving controlled and targeted delivery of therapeutic agents like VEGF. These DDS are classified as nanocarriers (NCs), an emerging method involving the encapsulation of active pharmaceutical drugs into nano-sized carriers for diagnostic and therapeutic applications (32-34). Remarkably, NCs exhibit several advantageous properties for drug delivery, including protecting the encapsulated drug against systematic degradation, enhancing drug solubility, and minimizing tissue toxicity (34-36). Recently, biopolymer-based nanocarriers (NCs) have gained prominence as a compelling avenue for drug delivery. Among these, dextran, an adjustable acid-labile biopolymer, has garnered significant attention due to its favorable characteristics such as biocompatibility, biodegradability, and low immunogenicity (37-39). Additionally, NCs can offer site-specific targeting by either incorporating cell-specific receptors or trigger cargo release upon

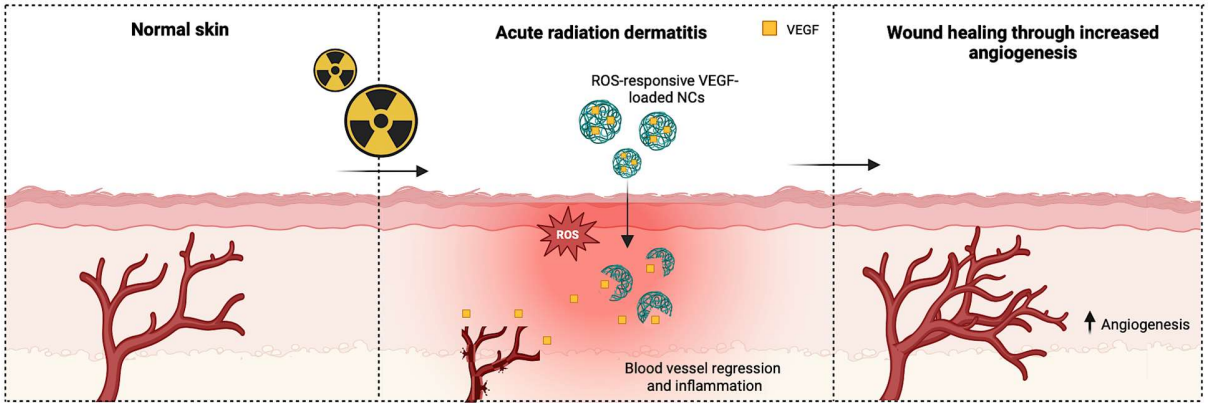

Figure 1: Drug delivery by ROS-responsive nanocarriers to promote wound healing in acute radiation dermatitis. *The pathophysiology of acute radiodermatitis, caused by radiotherapy, involves the formation of ROS, which subsequently causes blood vessel regression, the recruitment of immune cells, and inflammation. ROS-responsive nanocarriers could potentially cause targeted drug delivery of VEGF, promoting angiogenesis, to stimulate wound healing after radiotherapy. ROS, Reactive oxygen species; VEGF, Angiogenic vascular endothelial growth factor; NC, Nanocarrier.*

endogenous or exogenous stimuli such as ROS, glutathione, pH, enzymes, proteins, and temperature. Since radiation increases ROS levels in the skin, ROS-responsive NCs can be used as a targeted DDS in ARD (40-42). To achieve ROS responsiveness, thioketal moieties can be incorporated in the biopolymer to ensure a stimuli-induced release in the skin after irradiation. Currently, there are no treatments for RT-induced wounds using therapeutically loaded and bioresponsive NCs (43-45).

Here, we aim to test the ROS responsiveness of both rhodamine B- loaded NCs (Rho B) and VEGF-loaded NCs and evaluate the angiogenic potential of VEGF. Our research group has already successfully validated VEGF's ability to promote angiogenesis, making it an excellent candidate for NC cargo. To achieve the aim of this study, we focus on establishing an *in vitro* irradiation model using human umbilical vein endothelial cells (HUVECs) to mimic elevated ROS levels following RT. Subsequently, we evaluate both the ROS-responsiveness and angiogenic potential of VEGF-loaded NCs in this *in vitro* ROS model, crucial for confirming that VEGF retains its angiogenic efficacy upon release triggered by elevated ROS levels. The hypothesis states that NCs loaded with VEGF are ROS-responsive and will enhance angiogenesis in HUVECs upon NC cracking. Ultimately, this study will establish the groundwork for a novel, evidence-based therapeutic strategy using VEGF to mitigate the impact of ARD by enhancing radiation-induced wound healing. This approach will improve the comfort, well-being, and overall quality of life for cancer patients during and after RT treatment.

EXPERIMENTAL PROCEDURES

Nanocarrier synthesis and characteristics – In this study, we used dextran-based NCs composed of ROS-sensitive thioketal linkers loaded with VEGF or Rho B. The Rho B and VEGF-loaded NCs were redispersed in 0.3 wt% SDS water and had a solid content of 7.5 mg/ml and 6.9 mg/ml, respectively. Dynamic light scattering was used to obtain the hydrodynamic diameter, which measured 166 nm for the Rho B-loaded NCs and 179 nm for the VEGF-loaded NCs. The polydispersity index was 0.22 for both NCs.

Cells and Cell Culture – Human umbilical vein endothelial cells (HUVECs) were cultured in endothelial cell growth medium-2 (EGM-2) (Lonza Bioscience, CC-3162) supplemented with 10% fetal bovine serum (FBS). Cells were incubated at 37°C in a humidified atmosphere containing 5% CO_2, and the medium was changed every 3 days. For experiments, HUVECs between passages 6 and 9 were used. The proliferation assay, immunofluorescent (IF) staining, Fluorescence-Activated Cell Sorting (FACS), and Alamar Blue assay were conducted in a mixture of ½ endothelial cell growth basal medium-2 (EBM-2) (Lonza, Bioscience, CC-3156) and ½ EGM-2, supplemented with 0.25% FBS. The 2'-7'-

Dichlorohydrofluorescein diacetate (H_2DCFDA) assay was conducted in the phenol red-free mixture.

Alamar Blue assay – To assess cell viability HUVECs were seeded in 96-well plates ($2x10^3$ cells) and exposed to various tBHP concentrations (5, 50, 100, 200, and 500 µM) for 30 min., 1, 2, and 3h or treated with. Rho B-loaded NCs and VEGF-loaded NCs (5, 10, 50, 100, and 200 µg/mL) for 24, 48 and 72h. For the X-ray irradiation, cells were irradiated with 1, 10, and 20 Gray (Gy) with an X-ray irradiator (Xoft® Axxent® Electronic Brachytherapy (eBx®) System®). Unirradiated HUVECs that underwent the same handling and transportation as the irradiated cells were used as the negative control, while Milli-Q water was used as the positive control for cell death. A 10% Alamar Blue solution (Bio-Rad, BUF012A) was added to the cells and incubated for 4h on 37°C. Following incubation, cell supernatans was transferred to a black 96-well plate and fluorescence intensity was measured at excitation/emission 530/590 using the CLARIOstar^{Plus} (BMG Labtech). Data are expressed as the relative percentage of the negative control.

H_2DCFDA assay – To assess ROS levels, HUVECs were seeded in a black 96-well plate ($2x10^3$ cells) and treated with various concentrations of tBHP (5, 50, and 100 µM tBHP) for 3h or Rho B and VEGF-loaded NCs (5, 10, 50, 100, and 200 µg/mL) for 24, 48 and 72h or irradiated with 1, 10, and 20 Gy using an X-ray irradiator (Xoft® Axxent® Electronic Brachytherapy (eBx®) System®). Additionally, 50 µM and 100 µM tBHP were used as positive controls. Prior to the treatment, cells were incubated with 10 µM H_2DCFDA for 30 min. Excess H_2DCFDA was removed by washing, and fluorescence was detected at excitation/emission wavelengths of 485/535 nm using the CLARIOstar^{Plus} (BMG Labtech) platereader. The fluorescent H_2DCFDA signal was corrected for the number of cells. For this purpose, cells were incubated with Trichloroacetic acid-sulforhodamine B (TCA-SRB) (0.004% w/v SRB in 10% w/v TCA) (2-8 °C) for 15 min. at 4 °C. Unbound SRB was removed by washing with 1% acetic acid and the acidic ph was neutralized by 10 mM Trizma base. Fluorescence intensity was measured by the CLARIOstar^{Plus} (BMG Labtech) plate reader with excitation/emission of 565/586 nm. Data are represented as a ratio of DCF/SRB.

IF staining – HUVECs were seeded on coverslips in 24-well plates ($15x10^3$cells) and treated for 24h with Rho B-loaded NCs (50 and 100 µg/mL). Cells were first fixed with 4% paraformaldehyde (PFA) for 20 min. at room temperature (RT). Next, cells were incubated for 10 min. with Wheat germ agglutinin 647 (WGA647) (MERGR, W32466) and 4′,6-diamidino-2-phenylindole (DAPI) (1 mg/mL, Thermo Fisher) at RT. Cells were wash with 1X Phosphate Buffered Saline (PBS) between each incubation step. Finally, cells were mounted with Fluorescence Mounting Medium (Dako) on microscope slides for imaging with the LSM 900 confocal microscope (Zeiss). The ZEN Blue software (Zeiss) was used to analyze the data. The images of the samples were acquired in z-stack mode.

FACS – To assess ROS levels after tBHP treatment, HUVECs were seeded in 12 well plates ($80x10^3$ cells) and treated with 5, 50, and 100 µM tBHP for 3h. To assess NC colocalization, HUVECs were seeded in 12 well plates ($80x10^3$ (24h) and $50x10^3$ (6, 4, and 2h) cells) and treated with Rho B-loaded NCs (50 and 100 µg/mL) for 2, 4, 6, and 24h. For all experiments, untreated cells served as a negative control. To halt treatments, cells were washed with PBS, trypsinized, and centrifuged at 2000rpm for 5 min. at 20°C. Cells were washed with FACS buffer (PBS with 2% FBS) and centrifuged at 2000rpm for 5 min. at 20°C. For the NC experiments, cells were fixed in 1% PFA at 4°C overnight and the fluorescents signal was detected with BD LSRFortessaTM cell analyzer. Data analysis was performed using FlowJo.

Ellman's reagent assay – To measure reduced glutathione, an Ellman's reagent assays was performed. HUVECs were seeded in 6-well plates ($120x10^3$ cells) and treated with 5, 50, and 100 µM tBHP for 24h. cells were trypsinized, washed, and centrifuged at 300 x g for 5 min. Cells were resuspended in cold radioimmunoprecipitation assay (Roche, 04693159001) buffer, incubated on ice for 20 min., and centrifuged again. To remove the proteins, the supernatant was incubated with 100% TCA (Fisher scientific, 11964064) for 30 min. on ice, and centrifuged at 14,000 x g for 15 min. at 4°C. The supernatant was collected and incubated with 5,5'-dithio-bis-2-nitrobenzoic acid (ThermoFisher, 22582), Ellman's reaction buffer

(0.1M sodium phosphate (pH 8.0) containing 1 mM EDTA), and the reduced glutathione standard or samples for 15 min. at RT. Absorbance was measured using the CLARIOstar Plus (BMG Labtech) plate reader with excitation/emission of 565/586 nm. Samples were then incubated with 2 mM TCEP for 5 min. at RT, and the assay was repeated.

RNA extraction and quantitative polymerase chain reaction (qPCR) – To measure the gene expression of superoxide dismutase 1 (SOD1), superoxide dismutase 2 (SOD2), catalase (CAT), glutathione peroxidase 1 (gpX1), glutathione peroxidase 4 (gpX4), glutathione reductase (Gr), nuclear factor erythroid 2-related factor 2 (NRF2), and NAD(P)H quinone oxidoreductase 1 (NQO1), qPCR was performed in which HUVECs were seeded in 6-well plates ($120x10^3$ cells) and treated with 5, 50, and 100 µM tBHP for 24h. For total mRNA extraction, samples were treated with chloroform for 5 min., following centrifugation for 15 min. at 4°C at 14000 RPM and incubation with glycogen. The aqueous phase was collected and incubated with 2-isopropanol for 30 min. Next, samples were centrifugated for 10 min. at 4°C at 14000 RPM, the supernatant was removed, washed with 75% cold ethanol, and dissolved in water (Milli-Q). Next, mRNA concentration and quality were validated using Nanodrop ND-2000 spectrophotometer (Isogen Life Science, De Meern, The Netherlands). Hereafter, 3 ng/ul cDNA samples were synthesized using a T-100 Thermal cycler (Biorad, California, USA) and Qscript (Quantabio, Massachusetts, US). Eventually, a PCR master mix was prepared containing qPCR SYBR Green (thermo fisher scientific, Waltham, USA), primer pairs (supplementary table 1), and samples. Cycle conditions were: 95°C, 20'' [95°C, 3''- 60°C, 30'']40x – 95°C, 15'' – 60°C, 60'' – 95°C, 15s. Fold change was calculated from Ct values- and normalized to validated housekeeping genes YWHAZ and CYCA (GeNorm software).

ELISA – To observe the release of VEGF, VEGF-loaded NCs were incubated with cell conditioned medium (CCM; medium incubated with HUVECs for 3 days), blank conditioned medium (BCM; medium incubated without HUVECs for 3 days), 10 mM H_2O_2, and water (MiliQ) for 1, 2, 3, 6, 19, and 24h on 37°C. To assess the effect of dextranase on VEGF stability, 20 ng/mL VEGF was incubated with 250 µg/mL dextranase, 10 mM H_2O_2, 250 µg/mL dextranase with 10 mM H_2O_2, and PBS for 14h, 24h, and 5 days on 37°C. Additionally, 20 ng/mL freshly prepared VEGF (0h) was incubated with PBS. To investigate whether dextranase could enhance VEGF release, VEGF-loaded NCs were incubated with BCM, CCM with 10 mM H_2O_2 or dextranase 250 µg/mL or 10 mM H_2O_2 and dextranase 250 µg/mL for 3, 8, 20, and 26h on 37°C. All assays were performed according to the manufacture's guidelines ((BioLegend, 446504).

Proliferation assay – To examine whether VEGF retains its angiogenic effect post-irradiation, HUVECs were seeded in 96-well plates ($2x10^3$ cells) and irradiated with 2, 5, and 10 Gy using an X-ray irradiator (Xoft® Axxent® Electronic Brachytherapy (eBx®) System®). Afterwards, HUVECs were treated with 20 ng/mL VEGF for 24, 48, and 72h. untreated irradiated and non-irradiated cells were used as a negative control. Images were captured every 2h for 72h at 10x magnification using the Incucyte S3 Live-Cell system (Sartorius). Data analysis was performed using the Incucyte Analysis Software.

Statistical analysis – The statistical analysis was carried out using GraphPad Prism 10 (GraphPad Software, version 10.5.1). All data are presented as the mean ± Standard Error of the Mean (S.E.M). Normality was checked using the Shapiro-Wilk test. One-way ANOVA was used for continuous data with one independent variable, and two-way ANOVA for two independent variables, with Dunnett's test for multiple comparisons. If outliers were detected, a mixed-effect analysis was performed. ***P<0.0001, **P<0.001, *P<0.01.

RESULTS

tBHP served as an efficient ROS inducer while preserving cell viability - In this study, we first aimed to optimize a positive control for ROS production in HUVECs to facilitate further ROS experimentation *in vitro*. For this purpose, tert-butyl hydroperoxide (tBHP) was selected due to its capability to induce ROS generation in various cellular systems, such as hepatocytes and endothelial cells via lipid peroxidation and protein oxidation (46, 47). An ideal positive control for ROS production maximizes ROS levels without inducing cytotoxicity. To evaluate the cell viability upon tBHP treatment, an Alamar Blue assay was performed. HUVECs were exposed to various

concentrations of tBHP (5, 50, 100, 200, 500µM) for 1, 2, and 3h. (Fig 2a). Our results show that 5 and 50 µM tBHP did not induce cell death. Conversely, 200 and 500 µM tBHP significantly induced high levels of cell death across all time periods. Specifically, 200 µM tBHP decreased cell viability to 42% after 3h, while 500 µM tBHP reduced cell viability to 25%. Moreover, exposure to 100 µM tBHP resulted in significant, yet less extensive, cell death with a cell viability of 78% after 3h. Consequently, due to the high levels of cytotoxicity observed, concentrations of 200 and 500 µM tBHP were excluded from further experiments and were not used as positive controls for ROS production.

Following cytotoxicity evaluation, ROS production induced by tBHP was assessed by an H_2DCFDA assay. HUVECs were exposed to various concentrations of tBHP (5, 50, 100µM), and ROS production was monitored as a 3h timelapse using a plate reader. The results showed that treatment with 5 µM tBHP did not produce higher ROS levels compared to the negative control (0.11). However, treatment with 50 µM tBHP and 100 µM tBHP resulted in higher ROS levels of 0.28 and 0.24, respectively (Fig. 2b). To validate the ROS production by tBHP, FACS was performed on HUVECs treated with various tBHP concentrations (5, 50, 100µM) for 3h. Consistent with the plate reader results, the FACS data showed an increase in DCF fluorescent intensity and DCF-positive cells with increasing tBHP concentrations compared to the control group (Fig. 2c-d). To conclude, our data indicates that the concentration of 50 µM tBHP emerges as the optimal choice for inducing significant ROS production without eliciting cytotoxic effects, thus positioning it as the preferred positive control for subsequent ROS experiments.

To investigate the oxidative stress response of HUVECs following ROS induction by tBHP, qPCR and Ellman's reagent assays were performed. The Ellman's reagent assay was conducted to gain insight into the balance between reduced glutathione (GSH) and its oxidized form, glutathione disulfide (GSSG). This balance is a critical mechanism in the antioxidant system of the cell. Specifically, reduced GSH is essential for neutralizing cellular ROS by undergoing oxidation to GSSG (48). The Ellman's reagent assay measures the amount of cellular reduced GSH. For this, HUVECs were treated with various concentrations of tBHP (5, 50, and 100 µM) for 24h. The results demonstrated a concentration-dependent increase in the amount of reduced GSH with increasing tBHP concentrations (Fig. 2e). Control cells exhibited a baseline level of 0.4 µM reduced GSH. Treatment with 5, 50, and 100 µM tBHP resulted in increased levels of reduced GSH to 5, 61, and 101 µM, respectively. Furthermore, the Ellman's reagent assay was repeated on the same samples (HUVECs treated with 5, 50, and 100 µM tBHP for 24h) after treatment with 2 mM of TCEP, a substance that converts GSSG into its reduced GSH form by breaking disulfide bonds present in GSSG. Using TCEP allows for the measurement of the total cellular pool of GSH, as TCEP reduces all cellular GSSG to GSH (49, 50). The results of the Ellman's assay indicated that the total pool of GSH present in the different samples was approximately the same, with concentrations of approximately 210 µM for the untreated control, 198 µM in the 5 µM tBHP sample, 201 µM in the 50 µM tBHP sample, and 203 µM in the 100 µM tBHP sample (Fig. 2e). Additionally, we calculated the amount of GSSG by subtracting the amount of reduced GSH from the total GSH pool since the total pool of GSH in the cell comprises both reduced GSH and GSSG. These calculations showed that the control cells exhibited a baseline level of 209 µM GSSG. Treatment with 5, 50, and 100 µM tBHP resulted in decreased levels of GSSG to 193, 140, and 102 µM, respectively. conclusion, our findings suggest that increasing tBHP concentrations increases cellular reduced GSH levels and decreases GSSG amount. Furthermore, we used qPCR to assess the expression levels of key antioxidant genes (SOD1, SOD2, CAT, gpX1, gpX4, Gr, NRF2, and NQO1) after treating the cells with 5, 50, and 100 µM tBHP for 3h. This was done to determine if these genes were upregulated, indicating activation of the cell's antioxidant mechanism. Our findings revealed a concentration-dependent effect in the expression of SOD1, Gr, NRF2, and NQO1, with higher mRNA levels correlating with increasing tBHP concentration (Fig. 2f). At 100 µM tBHP, SOD1 and SOD2 mRNA levels showed approximately 1.2- and 1.4-times higher expression, respectively. Gr mRNA expression was 2 times higher, while the expression of NRF2 and NQO1 exhibited approximately 1.5- and 1.9-times increases, respectively, following

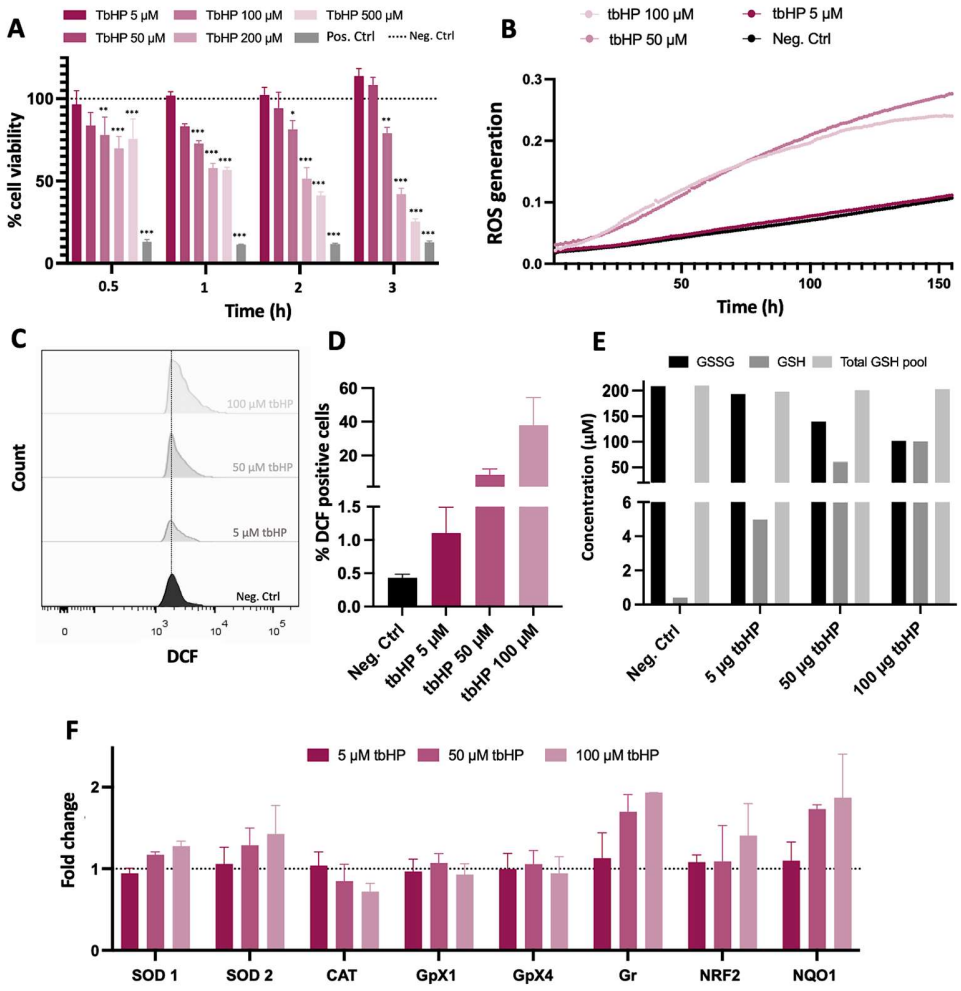

Figure 2: tBHP Induces cellular redox changes and cell death at high concentrations. ***(A)*** *Alamar Blue cell viability assay of HUVECs treated with different concentrations of tBHP (5, 50, 100, 200, 500 µM) for 1, 2, and 3h. Concentrations of 100, 200, and 500 µM tBHP induced high levels of cell death across all time periods, whereas 5 and 50 µM tBHP did not affect cell viability. Data is normalized to the untreated control (dotted line) and Milli Q was used as a positive control for cell death. n=3.* ***(B)*** *The intracellular ROS generation measured by the H_2DCFDA assay. the fluorescence intensity of DCF is measured in a timelapse of 3h after incubating HUVECs with different concentrations of tBHP (5, 50, 100, 200, 500 µM). Treatment with 5 and 50 µM tBHP caused an increase in ROS levels compared to the control. Untreated cells were used as the negative control. n=1.* ***(C)*** *DCF fluorescent signal measured by FACS, after tBHP treatment (5, 50, and 100 µM) for 3h. Vertical line represents the fluorescent intensity of the untreated control.* ***(D)*** *Percentage of DCF positive cells after tBHP treatment (5, 50, and 100 µM) for 3h, measured by FACS. The percentage H_2DCFDA positive cells increased over time. n=2. (E) Ellman's reagent assay of HUVECs treated with different concentrations of tBHP (5, 50, 100, 200, 500 µM) for 24h. The data represents concentration of oxidized glutathione (GSSG), reduced glutathione (GSH), and the total GSH pool in the cell. The data shows an increase in reduced GSH and decrease in GSSG with increasing tBHP concentrations. Untreated cells served as the negative control. n=1.* ***(F)*** *Gene expression levels of antioxidant genes (SOD1, SOD2, CAT, GPX1, GPX4, NRF2, and NQO1) in HUVEC treated with different concentrations of tBHP (5, 50, and 100 µM) for 3h. Data shows an increasing trend in SOD1, SOD2, Gr, NRF2, and NQOP1 gene expression with higher tBHP concentrations. n=2. Data are represented as mean ± SEM. ***P<0.0001, **P<0.001, *P<0.01, as determined by two-way ANOVA followed by Dunnett's multiple comparisons test* ***(A, D)***. SOD1, superoxide dismutase 1; SOD2, superoxide dismutase 2; CAT, catalase; gpX1, glutathione peroxidase; pgX4, glutathione peroxidase; Gr, glutathione reductase; NRF2, nuclear factor erythroid 2-related factor 2, NQO1, NAD(P)H quinone oxidoreductase.

treatment with 100 µM tBHP. In contrast, CAT mRNA levels decreased with increasing tBHP levels, while GpX1 and GpX4 mRNA levels remained relatively stable across all tBHP concentrations tested. In conclusion, our findings suggest that increasing tBHP concentrations induce higher oxidative stress in HUVECs, which in turn prompts an upregulation of antioxidant gene expression, including SOD1, Gr, NRF2, and NQO1.

ROS-responsive Rho B- and VEGF-loaded nanocarriers do not induce cytotoxicity at low concentrations - For NCs to be deemed appropriate as a safe DDS for preclinical, translational, and clinical studies, it is imperative that they demonstrate non-toxicity within a cellular environment. For this purpose, we investigated whether Rho B and VEGF-loaded NCs exhibit a cytotoxic effect on HUVECs using an Alamar Blue assay. The results indicate that low concentrations of Rho B-loaded NCs (5, 10, 50, and 100 µg/ml) and VEGF-loaded NCs (5, 10, and 50 µg/ml) exhibited no toxicity in HUVECs over a 72h period (Fig. 3a and 1b). However, treatment with 200 µg/ml of Rho B-loaded NCs notably decreased cell viability. Following exposure to this concentration, cell viability decreased to 30% after 24h, further dropping to 15% after 48 and 72h. In comparison, treatment with both 100 µg/ml and 200 µg/ml of VEGF-loaded NCs resulted in decreased cell viability. Specifically, treatment with 100 µg/ml decreased cell viability to 80% after 24 and 48h, while at a concentration of 200 µg/ml, cell viability dropped to 10% after 24h. These results indicate that low concentrations of NCs, do not induce cytotoxicity in HUVECs. Moreover, there is a noticeable decrease in cell viability with higher and longer treatments, indicating a concentration and time-dependent decline.

HUVECs effectively take up Rho B-loaded NCs - Following the cell viability study, subsequent experiments were conducted to investigate the uptake of Rho B-loaded NCs by HUVECs. Initially, NC colocalization with HUVECs was assessed via FACs analysis. HUVECs were exposed to the highest non-toxic concentration of Rho B-labeled NCs (100 µg/mL) for varying durations (2, 4, 6, and 24h). The results demonstrated a time-dependent increase in Rho B fluorescent intensity within HUVECs compared to the untreated control, with peak fluorescence intensity rising as the duration of NC incubation increased (Fig 3c). Furthermore, the percentage of Rho B-positive cells significantly increased with prolonged incubation times (Fig. 3d), rising from 74% at 2h to 98% at 24h, compared to the negative control. To ensure that the NCs were not adhering to the cell membrane, NC internalization was evaluated using an IF staining performed with the confocal microscope in Z-stack mode. For this purpose, HUVECs were treated with 100 µg/mL of Rho B-loaded NCs for 24h. Results show that Rho B-loaded NCs were internalized by HUVECs and were located in proximity of the cell nucleus (Fig. 3e, white arrows). Collectively, these data suggest that the NCs are effectively internalized by HUVECs.

Rho B- and VEGF-loaded NCs do not induce cellular stress - To evaluate the impact of NC treatment on oxidative stress levels in HUVECs, an H_2DCFDA assay was conducted. HUVECs were treated with various concentrations of both Rho B- and VEGF loaded NCs (10, 50, 75, 100, and 100 µg/mL) for 24, 48, and 72h. The results indicate that neither Rho B-loaded nor VEGF-loaded NCs tended to increase the ROS levels compared to the negative control after 24h (Fig 3h and 3i). Subsequent treatment with both NCs showed a tendency for a minor increase in ROS generation after 48 and 72h; however, this elevation was minimal and did not reach substantial levels. Notably, despite the prior optimization of the positive control for ROS production, it too showed no significant increase in ROS levels compared to the untreated control. Overall, these findings suggest that both NCs tend to induce only a modest elevation in ROS production, which is not pronounced.

Dextranase enhances the release of VEGF from VEGF-loaded NCs *in vitro* - Furthermore, we aimed to evaluate the responsiveness and VEGF release from our VEGF-loaded NCs. To achieve this, we conducted *in vitro* experiments in which the particles were treated with the ROS molecule H_2O_2 to examine both the responsiveness and the amount of VEGF released. Demonstrating the efficient VEGF release from NCs upon exposure to ROS molecules, confirms their potential as drug delivery system to release VEGF in a controlled and targeted manner for therapeutic use in ARD. To evaluate the VEGF release from ROS-responsive NCs, the NCs were incubated with cell conditioned medium (CCM; medium incubated with HUVECs for 3 days), blank conditioned medium (BCM; medium incubated without HUVECs for 3 days), 10 mM H_2O_2, and water for 1, 2, 3, 6, 19, and 24h.

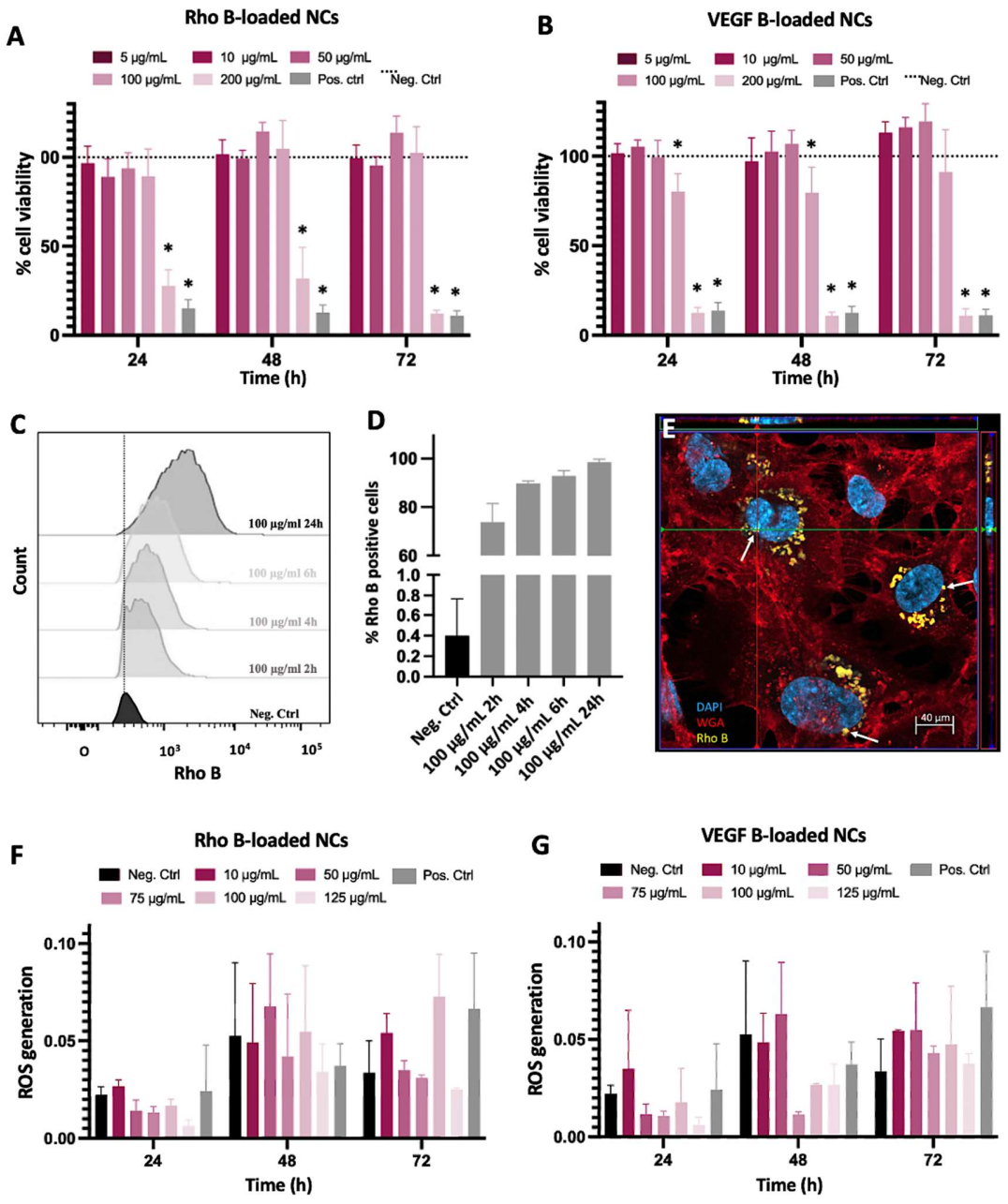

Figure 3: Rho B-loaded NCs are biocompatible, taken up by HUVECS, and do not induce cellular stress. (A, B) *Alamar Blue cell viability assay of HUVECs treated with different concentrations of Rho B-loaded NCs* ***(A)*** *and VEGF-loaded NCs* ***(B)*** *(5, 10, 50, 100, and 200 µg/mL) for 24, 48, and 72h. HUVECs exhibited reduced cell viability with 200 µg/mL of Rho B-loaded and VEGF-loaded NCs across all incubation times, and with 100 µg/mL of VEGF-loaded NCs for 24 and 48h. Data is normalized to the untreated control (dotted line) and Milli Q was used as a positive control for cell death. n=3.* ***(C)*** *Percentage of Rho B positive cells after treatment with 100 µg/mL Rho B-loaded NCs for 2, 4, 6, and 24h, measured by FACS. The percentage Rho B positive cells increased significantly over time. Data is normalized to the untreated control (Neg. Ctrl). n=2.* ***(D)*** *Rho B fluorescent signal measured by FACS after 100 µg/mL Rho B-loaded NC treatment for 24h. Vertical line represents the fluorescent intensity of the untreated control.* ***(E)*** *Representative Z-stack image of HUVECs treated with 100 µg/mL Rho B-loaded NCs for 24h. Nuclei (DAPI, blue), cell membrane (WGA, red), and Rho B NCs (yellow). Image shows Rho B NC internalization by HUVECs (white arrow). Scale bar: 40µm.* ***(F, G)*** *HUVEC intracellular ROS detection by H_2DCFDA assay after 24, 48 and, 72h of treatment with different concentration of Rho B-loaded NCs (10, 50, 75, 100, 125 µg/mL)* ***(F)*** *and VEGF-loaded NCs (10, 50, 75, 100, 125 µg/mL)* ***(G).*** *ROS levels tend not increase after 24h with Rho B and*

The release of VEGF determined using an ELISA assay and our results showed a 0.01 ng/ml VEGF release after 1h incubation with water, 10 mM H_2O_2, and CCM (Fig 4a). Notably, incubation with BCM showed a higher VEGF release (0.039 ng/mL). These findings suggest that the levels of ROS in the CCM were insufficient to crack the NCs. Furthermore, H_2O_2 was not effective in breaking down the NCs compared to water.

To enhance the VEGF release from the NCs, we employed dextranase, an enzyme that degrades dextran, to facilitate the cracking of NCs and subsequent VEGF release. This approach was chosen based on previous studies that demonstrated the effectiveness of dextranase in promoting the degradation of dextran-based materials (7, 8). Before proceeding with this approach, we first evaluated whether dextranase could adversely affect VEGF stability. Given that dextran requires a temperature of 37°C for optimal functionality, all samples were incubated at this temperature. An ELISA was conducted using 20 ng/mL VEGF, incubated with either 250 µg/mL dextranase, 10 mM H_2O_2, or a combination of 250 µg/mL dextranase with 10 mM H_2O_2, and PBS for 14h, 24h, and 5 days. Additionally, the amount of freshly prepared VEGF (0h) in PBS was also detected. Our results show that at 0h, the initial VEGF concentration in PBS is 1.83 ng/mL and further declines to 0.32 ng/mL at 14h (Fig S1), indicating rapid VEGF degradation, likely influenced by RT. Furthermore, VEGF levels were lower in the dextranase-treated group (0.1 ng/mL) compared to the PBS control group (0.32 ng/mL) (Fig. 4b). From 14h to 5 days, all groups showed a similar trend of decreasing VEGF levels. These data suggest a modest negative impact of dextranase and temperature on VEGF stability and bioactivity.

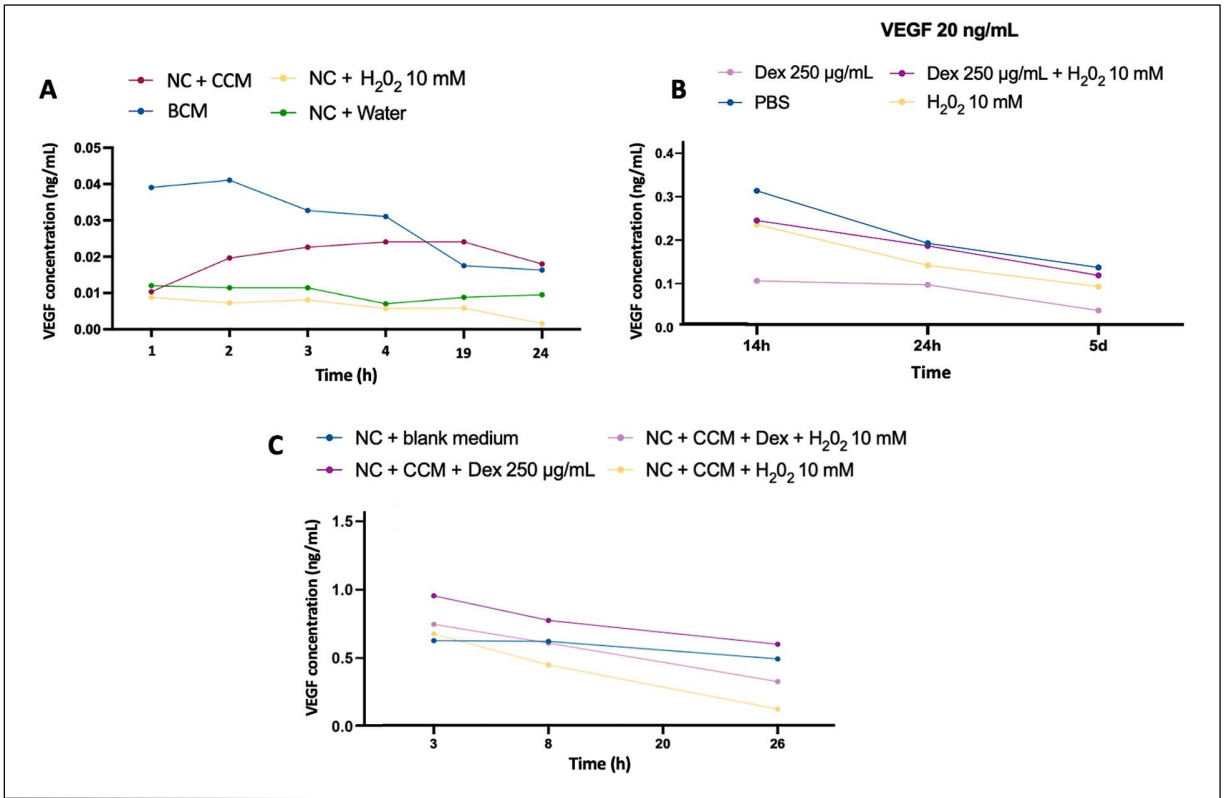

Figure 4: Dextranase enhances VEGF release from VEGF-loaded NCs in presence of H_2O_2, despite negative impact on VEGF stability. (A) *VEGF concentration released from VEGF-loaded NCs exposed to cell conditioned medium (CCM; medium incubated with HUVECs for 3 days), blank conditioned medium (BCM; medium incubated without HUVECs for 3 days), 10 mM H_2O_2, and water for 1, 2, 3, 6, 19, and 24h, de. Data suggests no large differences in the VEGF release between the conditions.* ***(B)*** *VEGF concentration after 20ng/mL VEGF was incubated with 250 µg/mL dextranase, 10 mM H_2O_2, 250 µg/mL dextranase with 10 mM H_2O_2, and PBS for 14h, 24h, and 5 days. VEGF levels were lower in the groups treated with dextranase, H_2O_2, and their combination compared to the PBS control group.* ***(C)*** *VEGF concentration released from VEGF-loaded NCs incubated with BCM, CCM with 10 mM H_2O_2 or dextranase 250 µg/mL or 10 mM H_2O_2 and dextranase 250 µg/mL for 3, 8, 20, and 26h. Data shows a slight increase in released VEGF upon the presence of dextranase and dextranase with H_2O_2 compared to the group solely exposed to H_2O_2. CCM, conditioned medium; BCM, blank conditioned medium; Dex, Dextranase.*

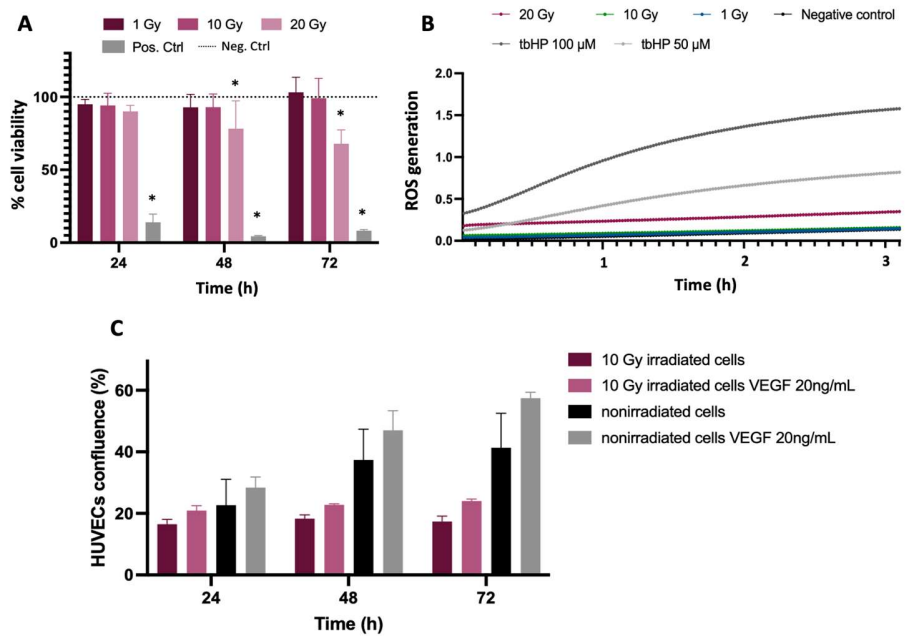

Figure 5: 10 Gy of X-ray irradiation cause elevated ROS, reduce cell viability, and negatively impact VEGF stability. ***(A)*** *Alamar Blue cell viability assay of HUVECs exposed to low energy X-ray irradiation at doses of 1, 10, and 10 Gy. Cell viability was measured 24, 48 and 72h after exposure. Data shows no cytotoxicity at 1 and 10 Gy, while 20 Gy led to a significant decrease in cell viability. Data is normalized to the negative control (dotted line) and Milli Q was used as a positive control for cell death. n=2.* ***(B)*** *The intracellular ROS generation measured by the H_2DCFDA assay. The DCF fluorescence intensity is measured over a timelapse of 3h after exposure of HUVECs to low energy X-ray irradiation at doses of 1, 10, and 10 Gy. HUVECs irradiated with 10 Gy tend to produce higher ROS levels compared to the negative control, while irradiation with 10 and 1 Gy did not show elevated ROS production. n=2.* ***(C)*** *HUVECs confluence was measured using a proliferation assay after exposure to low energy X-ray irradiation of 10 Gy and subsequent treatment with 20 ng/ml of VEGF for 72h. The data indicates that, even post-irradiation, VEGF caused a slight promotion of cell proliferation, albeit at a reduced level compared to nonirradiated cells. n=1. All data are represented as mean ± SEM. *P<0.0001 as determined by two-way ANOVA followed by Dunnett's multiple comparisons test* ***(A).***

Following this experiment, we investigated whether dextranase could enhance VEGF release from the NCs. For this purpose, the VEGF release was quantified by ELISA on supernatant from NCs exposed to four distinct media conditions (BCM, CCM with 10 mM H_2O_2 or dextranase 250 µg/mL or 10 mM H_2O_2 and dextranase 250 µg/mL) for 3, 8, 20, and 26h. Our findings demonstrate a slightly higher release of VEGF upon the presence of dextranase (1.2 ng/mL VEGF) and dextranase with H_2O_2 (0.9 ng/mL VEGF) compared to the group solely exposed to H_2O_2 (0.8 ng/mL VEGF) (Fig. 4c). Furthermore, from 3h to 26h, there was a decreasing trend of VEGF among all groups. Conclusively, these results suggest that dextranase has the potential to augment the release of VEGF from the NCs.

Development of an *in vitro* model that mimics ARD - Following radiotherapy, the skin experiences heightened levels of ROS, leading to significant damage to both the skin and its blood vessels. The goal is to simulate this phenomenon by establishing an *in vitro* ARD model. This model will aid in assessing the ROS responsiveness of VEGF-loaded NCs and the angiogenic potential of the released VEGF, thereby enabling a better observation of the particles and the potential of VEGF in ARD. To accomplish this, HUVECs were exposed to low energy X-ray irradiation at doses of 1, 10, and 20 Gy, followed by the measurement of ROS levels using a H_2DCFDA assay. Our results show that HUVECs irradiated with 20 Gy produce higher ROS levels compared to the nonirradiated negative control, while irradiation with 10 and 1 Gy did not result in elevated ROS production (Fig. 5a). Subsequently, an Alamar Blue assay was performed to assess the cell viability of HUVECs irradiated with 1, 10, and 20 Gy (Fig. 5b). Our results revealed no cytotoxicity at 1 and 10 Gy after 24h. However, 20 Gy irradiation led to a significant decrease in cell viability, dropping to 78% at 48h and 67% at 72h compared to the nonirradiated negative control. Additionally, we investigated

whether transporting HUVECs in a 37°C box, without 5% CO_2, to the irradiation device influenced cell viability. Our results indicated that there was no effect on cell viability of the HUVECs due to the transport (Fig. S2). In conclusion, these findings indicate that 20 Gy irradiation induces toxicity in HUVECs.

We further aimed to investigate whether irradiation of the cells would influence the capacity of VEGF to promote proliferation. Assessing the impact of irradiation on the efficacy of VEGF in promoting HUVEC proliferation enables us to evaluate the effectiveness and reliability of our approach in stimulating cell proliferation after VEGF release for the NCs, despite potential structural alterations in HUVECs. To achieve this, HUVECs were exposed to low-energy X-ray irradiation at 10 Gy, followed by treatment with VEGF (20 ng/mL). Subsequently, we assessed cell proliferation over a period of 72h. We observed that administration of VEGF after irradiation resulted in a slightly higher increase in cell confluence compared to the irradiated untreated cells over the 72h period. However, it is important to note that this increase in proliferation was very minimal (Fig. 5c). Moreover, the proliferation capacity of irradiated HUVECs was lower than that of the unirradiated cells. VEGF treatment of unirradiated cells caused a much stronger increase in proliferation of HUVECs compared to the irradiated cells over the 72h period. The same trend was observed for irradiation at 2 Gy (Fig. S3a) and 5 Gy (Fig. S3b). The capacity of VEGF to promote proliferation was higher at 5 Gy and even greater at 2 Gy compared to 10 Gy, indicating a dose-dependent effect. In conclusion, these results indicate that irradiation has a negative impact on cell proliferation in general and on the efficacy of VEGF in promoting cell proliferation.

DISCUSSION

Radiation therapy (RT) is a common cancer treatment but often causes adverse inflammatory skin reactions such as ARD (3). Due to the lack of consensus on therapy, evidence-based treatment strategies are urgently needed to improve the healing of RT-induced wounds (7-10). Nanomedicine has recently gained popularity for its ability to protect drugs against *in vivo* degradation and deliver them precisely to targeted sites, enhancing therapeutic efficacy and reducing toxicity (34-36). RT induces ARD by damaging blood vessels and generating ROS, which harms the skin. Growth factors that promote angiogenesis are crucial for mitigating these effects (20, 21, 24, 51). This study aims to propose a new therapy for RT-induced wounds by examining the biocompatibility, uptake, and cellular stress effects of NCs, their responsiveness to ROS and subsequent VEGF release, and by creating and evaluating an *in vitro* ARD model.

First, we aimed to optimize tBHP as a positive control for ROS production. The Alamar Blue assay results showed no cytotoxicity in HUVECs at low tBHP concentrations (5 and 50 µM), while 200 and 500 µM tBHP induced significant cell death (52, 53). These findings align with previous studies, which reported no significant impact on cell viability with 50 µM tBHP, but notable reductions at 200 µM and higher, leading to necrosis. Our results also showed a significant reduction in cell viability at 100 µM tBHP, yet after 72h, average cell viability remained at 78%, close to the biocompatibility threshold of 80% (53-55).

However, it's important to consider the potential influence of cell passage on these findings. Older cells might exhibit reduced resilience to high ROS production compared to younger ones (56-58).

Furthermore, we investigated ROS levels in HUVECs using tBHP and an H2DCFDA assay with FACS. Concentrations of 50 µM and 100 µM tBHP significantly increased ROS levels compared to the control, consistent with previous studies (46, 53). Notably, 50 µM tBHP produced slightly higher ROS levels than 100 µM after 3h. Additionally, the Alamar Blue assay showed that 100 µM tBHP slightly decreased cell viability. The reduced ROS levels can be explained by the fact that dead cells produce less ROS due to ceased metabolic activity (60, 61). This contradicts our FACS results, where 100 µM tBHP induced higher ROS levels compared to 50 µM tBHP. Differences in cell passages might contribute to these discrepancies between the FACS and timelapse data. Younger cells, which have a more robust defense system against ROS due to higher antioxidant levels, can better recover from ROS damage (56-58). For instance, the cell passage used for the FACS analysis was #7, while younger cells were used for the H_2DCFDA assay, potentially explaining the data variation. In the FACS, we observed that even the negative control showed detectable ROS levels, which are normal for regular

cellular functions such as signal transduction, cell proliferation, and immune responses (62-64). Additionally, the FACS involved changing the medium condition from 10% to 0.25% FCS, a drastic reduction that likely caused a slight increase in ROS due to the immediate shock experienced by the cells (65-67).

To investigate the cell's antioxidant response to ROS, we performed an Ellman's reagent assay and qPCR to examine the antioxidant system. The Ellman's assay measured the total glutathione pool, including oxidized (GSSG) and reduced (GSH) glutathione levels, after treatment with 5, 50, and 100 µM tBHP. We observed a concentration-dependent increase in GSH and a decrease in GSSG with higher tBHP concentrations. However, these findings were unexpected, diverging from the anticipated outcome. Ordinarily, one would anticipate observing higher GSSG and lower GH levels with increasing ROS concentrations within the cell. This expectation arises from the understanding that elevated ROS levels lead to increased oxidation of GSH to GSSG for ROS removal (68-71). This is supported by literature; Unterluggauer et al. demonstrated that high tBHP concentrations induce the conversion of the predominant cellular reduced GSH to oxidized GSSG (72). However, cells contain enzymes like Gr that recycle GSH by converting GSSG back into GSH (73, 74). Upregulating Gr can increase the conversion of GSSG to GSH. Our qPCR data showed that Gr expression was twice as high in cells treated with 100 µM tBHP compared to the negative control, indicating that Gr is actively reducing GSSG to GSH. This explains the increased GSH and decreased GSSG levels observed in the Ellman's assay and suggests that the cell's antioxidant mechanism is combating the high ROS levels (75, 76).

Furthermore, the qPCR analysis showed a concentration-dependent increase in the expression of antioxidant genes SOD1, Gr, NRF2, and NQO1, with higher mRNA levels and rising tBHP levels, indicating active antioxidant responses against ROS. In contrast, CAT mRNA levels decreased with higher tBHP concentrations, while GpX1 and GpX4 mRNA levels remained stable across all tBHP concentrations. This suggests that some genes may initially increase expression in response to tBHP-induced oxidative stress as part of the early cellular response to counteract ROS accumulation, but the expression levels of these genes return to baseline or decrease as the stress persists or cellular signaling adapts (77-80). In our study, we measured gene expression only after 24h, possibly missing transient changes. The decline in CAT expression observed may be due to its critical role in the initial stages of antioxidant defense. In situations of oxidative stress, CAT rapidly converts H_2O_2 into water and oxygen to prevent ROS accumulation (81, 82). Other studies have also reported decreases in CAT expression in HUVECs (83). By measuring gene expression at a single time point, we may miss earlier transient changes in the cellular response. Conducting time-course experiments, monitoring gene expression at multiple time points after tBHP exposure, would offer a more comprehensive understanding of antioxidant gene expression dynamics in response to oxidative stress. This approach would also enable a better study of ROS kinetics and associated enzymes.

Furthermore, Rho B and VEGF-loaded NCs were tested for their effects on HUVECs, including cytotoxicity, ROS production, and cellular uptake. Maintaining safety for future in vivo use is crucial. Low concentrations of both NCs (5-100 µg/ml) showed no cytotoxicity, attributed to the biocompatible dextran in the NCs (84, 85). However, higher concentrations (200 µg/ml) exhibited cytotoxicity. Ferrer et al. revealed similar results in which cell viability of HUVECs was not affected when treated with 20 µg/ml dextran based nanogels for 24h. However, treatment with 200 µg/ml nanogels for 24h caused a significant cytotoxic effect (86). When NCs are internalized, mechanical stress and membrane deformations can lead to cell death (87, 88). Elevated NC concentrations may cause oxidative stress by overproducing ROS, damaging cellular components and resulting in cell death. Studies have shown increased ROS levels in HUVECs treated with silver NCs, leading to similar harmful effects (89, 90). Our results on the ROS production upon treatment with Rho B and VEGF-loaded NCs showed no large increase in ROS production. However, it is worth noting that we did not test concentrations of 200 µg/ml NCs on ROS production, since the Alamar Blue assay indicated that this concentration caused significant cell death in HUVECs. Therefore, further validation of ROS production with 200 µg/ml NCs should be carried out to better understand the role

of ROS in the observed cytotoxicity. Additionally, High NC concentrations can disrupt cellular homeostasis by creating an osmotic pressure imbalance, leading to cytotoxic effects (93).
Treatment with NCs occasionally slightly reduced cellular ROS levels compared to the untreated control. Yaqin et al. suggest this reduction may be due to ROS oxidizing thioketal linkers, potentially explaining the observed decrease in ROS following NC treatment (52). Additionally, our results indicated a minor increase in ROS generation after 48 and 72h of NC treatment. The ROS increase might be due to mitochondrial ROS production from ROS-induced apoptosis, which could be further investigated using MITOsox (94 - 97). The positive control showed lower ROS levels than during the optimization phase. This could be due to differences in cell viability and health, reagent age (H_2DCFDA), experimental conditions, and cell passage number which may have impacted ROS production (100). After the cell viability study, we evaluated the potential of Rho B-loaded NCs for drug delivery by assessing their cellular uptake. Z-stack images demonstrated effective uptake of NCs, positioning them near the cell nucleus. Coenen et al. also observed similar localization of dextran NCs near the nucleus in HUVECs, supporting our findings (91). FACS analysis revealed time-dependent colocalization of Rho B NCs by HUVECs, with the percentage of Rho B positive cells increasing to 98% after 24h. Other studies have reported high uptake of dextran-based nanocarriers by HUVECs (86, 101). This efficient uptake of dextran NCs may be attributed to reduced opsonization by proteins in the medium and decreased nonspecific hydrophobic interactions between the carrier and cell membranes caused by the present of dextran (102, 103). Nanoparticle size is crucial for cellular uptake. Suzuki et al. showed that smaller TiO2 NCs (20 nm) are internalized more than larger ones (250 nm)(46). Our NCs, at 179 nm, are optimal for uptake, as previous studies confirm efficient uptake of similar-sized NCs by HUVECs. Additionally, the zeta potential (-14 mV) of our NCs enhances their interaction with the cell membrane, improving uptake (104-106).

In the following phase of our investigation, we aimed to test our NCs responsiveness to H_2O_2. These NCs, primarily made of thioketal linkers, are designed to release VEGF upon ROS exposure (43-45, 107). Initially, VEGF-loaded NCs were exposed to various conditions, including H_2O_2, CCM, BCM, and water. Surprisingly, VEGF release remained consistent across all conditions, even higher in blank conditioned medium. This indicates that ROS levels in CCM were insufficient to trigger NC dissolution, suggesting low ROS production by HUVECs. This experiment effectively rules out any influence of HUVECs on NC cracking, crucial for optimal drug delivery. The inefficiency of H_2O_2 in cracking the NCs might be due to its low concentration (10 mM), insufficient for significant oxidative stress needed to trigger thioketal linker cleavage. However, other studies have demonstrated content release from H_2O_2-responsive NCs with just 1 mM H_2O_2 (109, 110). Another possibility is that the pores formed by H_2O_2 degradation of thioketal linkers are too small, since VEGF is a relatively large molecule (109). To boost VEGF release from the NCs, we used dextranase to enlarge the pores in their dextran shell (111-113). Before incorporating dextranase, we checked if it affected VEGF stability. VEGF was incubated with 250 µg/mL dextranase, H2O2, a combination of dextranase and H2O2, or PBS for 14h, 24h, and 5 days at 37°C. Results showed lower VEGF levels in the dextranase-treated group compared to PBS, suggesting dextranase and the incubation temperature modestly negatively affected VEGF stability. This can be explained by the fact that dextranase likely contains proteolytic enzymes that contribute to VEGF degradation (114). Additionally, VEGF is sensitive to temperature, and prolonged exposure at 37°C accelerates its degradation (110, 115). Treating freshly made VEGF with PBS showed a drastic decrease from 1.83 ng/mL to 0.32 ng/mL within 14 h. This rapid decline is consistent with VEGF's known short *in vivo* half-life of approximately 30 min. (30). Finally, we examined if dextranase could enhance VEGF release from the NCs by exposing them to BCM, CCM with 10 mM H_2O_2 or dextranase 250 µg/mL or 10 mM H_2O_2 and dextranase 250 µg/mL) for 3, 8, 20, and 26h. Results showed slightly higher VEGF release with dextranase and dextranase with H_2O_2 compared to H_2O_2 alone. Overall, these findings indicate that dextranase has the potential to boost VEGF release from the NCs. To enhance VEGF release from the NCs using dextranase, stabilizing VEGF is crucial to increase its half-life and maintain its functionality (116, 117). Bovine serum albumin

(BSA) is a potential stabilizer known for preserving proteins and drugs from degradation (118-120). Future experiments should focus on optimizing VEGF stabilization with buffers containing 1% BSA to ensure its efficacy and longevity in therapeutic applications.

In the final part of our research we aimed to create an in vitro model of ARD by exposing HUVECs to varying doses of X-ray irradiation. An effective *in vitro* ARD model should mimic the conditions of elevated ROS levels observed in vivo without inducing significant cytotoxicity. We found that only the 20 Gy dose induced significant cytotoxicity after 48 and 72h, while cell viability was unaffected after 24h. This aligns with existing research suggesting cell death in HUVECs occurs at 20 Gy and higher doses (121, 122). Cell viability at 24 hours post-irradiation was consistently high, even at the 20 Gy dose. This delay in cytotoxicity at 20 Gy indicates that the harmful effects of high-dose irradiation may take time to develop, likely due to ROS accumulation and subsequent cellular damage. These results confirm the accuracy of our model in replicating known radiation-induced cellular responses, particularly the dose-dependent cytotoxicity seen in HUVECs. This validation is essential for the credibility of our in vitro model in investigating ARD mechanisms. Furthermore, we investigated ROS production in HUVECs irradiated with 1, 10, and 20 Gy. Surprisingly, neither 1 Gy nor 10 Gy caused substantial ROS elevation. Even at 20 Gy, ROS increase was minimal. This suggests that the cytotoxicity at 20 Gy may not be solely due to ROS rise, hinting at other contributing mechanisms, such as DNA damage and mutations induced by irradiation (13). The disparity between ROS levels and cytotoxicity at 20 Gy points to a potential flaw in our model. While high irradiation doses cause significant cell damage, ROS levels remain low. One solution is to adopt fractionated irradiation, delivering the total dose in smaller fractions over multiple sessions (123). This approach allows cells to undergo periods of rest and recovery between radiation doses, reducing the overall cytotoxicity while potentially increasing ROS levels. The advantage of fractionated is that it mirrors the clinical practice in which cancer patients also get fractionated radiotherapy, making *in vitro* studies more relevant and translatable to the clinical setting (124). In addition, we investigated whether irradiation affects HUVEC proliferation stimulated by VEGF. By assessing HUVEC response to VEGF post-irradiation, we determine if VEGF, when released from the NCs, retains its pro-angiogenic function. HUVECs were irradiated with 2, 5, and 10 Gy. This choice mirrors clinical practice, where cancer patients typically receive fractionated doses, each around 2 Gy (124). We observed that 10 Gy irradiation negatively affected VEGF-induced HUVEC proliferation, consistent with findings by Kermani et al (125). Interestingly, they found that irradiation upregulated VEGF receptor 2 but demonstrated that pretreatment with VEGF165 could reverse this effect and enhance VEGF's ability to promote proliferation. This suggests that pretreating with VEGF165 could be a promising approach to counteract irradiation's negative impact on endothelial cell proliferation, suggesting a valuable direction for further research.

CONCLUSION

In summary, the experiments in this study highlight the potential of ROS-responsive VEGF-loaded NCs to enhance the healing of RT-induced wounds. Collectively, our results indicate that the optimization of the positive control for ROS was successful with 50 µM tBHP, as it induced high levels of ROS without causing any cell death. Moreover, tBHP treatment activated the antioxidant mechanism in HUVECs by increasing antioxidant gene expression and likely converting GSSG to reduced GSH for ROS oxidation. Additionally, both Rho B and VEGF-loaded NCs were biocompatible, efficiently taken up by HUVECs, and do not induce oxidative stress at low concentrations. The addition of dextranase increased the ROS responsiveness and subsequent release of VEGF from the NCs, enhancing their effectiveness. Moreover, X-ray irradiation at 20 Gy could potentially form a robust *in vitro* ROS model that mimics ARD, allowing further investigation of the NC ROS responsiveness and the effect of VEGF. Given these findings, this study offers a promising therapeutic potential of NCs as a drug DDS for administering VEGF to stimulate angiogenesis and wound healing at RT-induced injury sites. Future studies are necessary to further evaluate the therapeutic potential of VEGF-loaded NCs, aiming to confirm the safety and efficacy for the treatment of ARD.

REFERENCES

1. Baskar R, Lee KA, Yeo R, Yeoh KW. Cancer and radiation therapy: current advances and future directions. Int J Med Sci. 2012;9(3):193-9.
2. FitzGerald TJ, Bishop-Jodoin M, Laurie F, Lukez A, O'Loughlin L, Sacher A. Treatment Toxicity: Radiation. Hematol Oncol Clin North Am. 2019;33(6):1027-39.
3. Rosenthal A, Israilevich R, Moy R. Management of acute radiation dermatitis: A review of the literature and proposal for treatment algorithm. J Am Acad Dermatol. 2019;81(2):558-67.
4. Perreard M, Heutte N, Clarisse B, Humbert M, Leconte A, Gery B, et al. Head and neck cancer patients under radiotherapy undergoing skin application of hydrogel dressing or hyaluronic acid: results from a prospective, randomized study. Support Care Cancer. 2023;32(1):7.
5. Eda K, Uzer K, Murat T, Cenk U. The effects of enteral glutamine on radiotherapy induced dermatitis in breast cancer. Clin Nutr. 2016;35(2):436-9.
6. Gabros S, Nessel TA, Zito PM. Topical Corticosteroids. StatPearls. Treasure Island (FL) ineligible companies. Disclosure: Trevor Nessel declares no relevant financial relationships with ineligible companies. Disclosure: Patrick Zito declares no relevant financial relationships with ineligible companies.2024.
7. Hegedus F, Mathew LM, Schwartz RA. Radiation dermatitis: an overview. Int J Dermatol. 2017;56(9):909-14.
8. Finkelstein S, Kanee L, Behroozian T, Wolf JR, van den Hurk C, Chow E, et al. Comparison of clinical practice guidelines on radiation dermatitis: a narrative review. Support Care Cancer. 2022;30(6):4663-74.
9. Schmuth M, Wimmer MA, Hofer S, Sztankay A, Weinlich G, Linder DM, et al. Topical corticosteroid therapy for acute radiation dermatitis: a prospective, randomized, double-blind study. Br J Dermatol. 2002;146(6):983-91.
10. Omidvari S, Saboori H, Mohammadianpanah M, Mosalaei A, Ahmadloo N, Mosleh-Shirazi MA, et al. Topical betamethasone for prevention of radiation dermatitis. Indian J Dermatol Venereol Leprol. 2007;73(3):209.
11. Liu Y, Yang M, Luo J, Zhou H. Radiotherapy targeting cancer stem cells "awakens" them to induce tumour relapse and metastasis in oral cancer. Int J Oral Sci. 2020;12(1):19.
12. Baskar R, Dai J, Wenlong N, Yeo R, Yeoh KW. Biological response of cancer cells to radiation treatment. Front Mol Biosci. 2014;1:24.
13. Borrego-Soto G, Ortiz-Lopez R, Rojas-Martinez A. Ionizing radiation-induced DNA injury and damage detection in patients with breast cancer. Genet Mol Biol. 2015;38(4):420-32.
14. Zheng Z, Su J, Bao X, Wang H, Bian C, Zhao Q, et al. Mechanisms and applications of radiation-induced oxidative stress in regulating cancer immunotherapy. Front Immunol. 2023;14:1247268.
15. Kim W, Lee S, Seo D, Kim D, Kim K, Kim E, et al. Cellular Stress Responses in Radiotherapy. Cells. 2019;8(9).
16. Moloney JN, Cotter TG. ROS signalling in the biology of cancer. Semin Cell Dev Biol. 2018;80:50-64.
17. Liu J, Han X, Zhang T, Tian K, Li Z, Luo F. Reactive oxygen species (ROS) scavenging biomaterials for anti-inflammatory diseases: from mechanism to therapy. J Hematol Oncol. 2023;16(1):116.
18. Mittal M, Siddiqui MR, Tran K, Reddy SP, Malik AB. Reactive oxygen species in inflammation and tissue injury. Antioxid Redox Signal. 2014;20(7):1126-67.
19. Yu W, Tu Y, Long Z, Liu J, Kong D, Peng J, et al. Reactive Oxygen Species Bridge the Gap between Chronic Inflammation and Tumor Development. Oxid Med Cell Longev. 2022;2022:2606928.
20. Wijerathne H, Langston JC, Yang Q, Sun S, Miyamoto C, Kilpatrick LE, et al. Mechanisms of radiation-induced endothelium damage: Emerging models and technologies. Radiother Oncol. 2021;158:21-32.
21. Byun MR, Lee SW, Paulson B, Lee S, Lee W, Lee KK, et al. Micro-endoscopic In Vivo Monitoring in the Blood and Lymphatic Vessels of the Oral Cavity after Radiation Therapy. Int J Med Sci. 2019;16(11):1525-33.
22. Tahergorabi Z, Khazaei M. A review on angiogenesis and its assays. Iran J Basic Med Sci. 2012;15(6):1110-26.
23. Omorphos NP, Gao C, Tan SS, Sangha MS. Understanding angiogenesis and the role of angiogenic growth factors in the vascularisation of

engineered tissues. Mol Biol Rep. 2021;48(1):941-50.
24. Breuss JM, Uhrin P. VEGF-initiated angiogenesis and the uPA/uPAR system. Cell Adh Migr. 2012;6(6):535-615.
25. Przybylski M. A review of the current research on the role of bFGF and VEGF in angiogenesis. J Wound Care. 2009;18(12):516-9.
26. Banai S, Shweiki D, Pinson A, Chandra M, Lazarovici G, Keshet E. Upregulation of vascular endothelial growth factor expression induced by myocardial ischaemia: implications for coronary angiogenesis. Cardiovasc Res. 1994;28(8):1176-9.
27. Senger DR, Davis GE. Angiogenesis. Cold Spring Harb Perspect Biol. 2011;3(8):a005090.
28. Dudley AC, Griffioen AW. Pathological angiogenesis: mechanisms and therapeutic strategies. Angiogenesis. 2023;26(3):313-47.
29. Milkiewicz M, Ispanovic E, Doyle JL, Haas TL. Regulators of angiogenesis and strategies for their therapeutic manipulation. Int J Biochem Cell Biol. 2006;38(3):333-57.
30. Simon-Yarza T, Formiga FR, Tamayo E, Pelacho B, Prosper F, Blanco-Prieto MJ. Vascular endothelial growth factor-delivery systems for cardiac repair: an overview. Theranostics. 2012;2(6):541-52.
31. Beheshtizadeh N, Gharibshahian M, Bayati M, Maleki R, Strachan H, Doughty S, et al. Vascular endothelial growth factor (VEGF) delivery approaches in regenerative medicine. Biomed Pharmacother. 2023;166:115301.
32. Patra JK, Das G, Fraceto LF, Campos EVR, Rodriguez-Torres MDP, Acosta-Torres LS, et al. Nano based drug delivery systems: recent developments and future prospects. J Nanobiotechnology. 2018;16(1):71.
33. Afzal O, Altamimi ASA, Nadeem MS, Alzarea SI, Almalki WH, Tariq A, et al. Nanoparticles in Drug Delivery: From History to Therapeutic Applications. Nanomaterials (Basel). 2022;12(24).
34. Yang J, Jia C, Yang J. Designing Nanoparticle-based Drug Delivery Systems for Precision Medicine. Int J Med Sci. 2021;18(13):2943-9.
35. Ventola CL. The nanomedicine revolution: part 1: emerging concepts. P T. 2012;37(9):512-25.
36. Riehemann K, Schneider SW, Luger TA, Godin B, Ferrari M, Fuchs H. Nanomedicine--challenge and perspectives. Angew Chem Int Ed Engl. 2009;48(5):872-97.
37. Nitta SK, Numata K. Biopolymer-based nanoparticles for drug/gene delivery and tissue engineering. Int J Mol Sci. 2013;14(1):1629-54.
38. Wasiak I, Kulikowska A, Janczewska M, Michalak M, Cymerman IA, Nagalski A, et al. Dextran Nanoparticle Synthesis and Properties. PLoS One. 2016;11(1):e0146237.
39. Ramasundaram S, Saravanakumar G, Sobha S, Oh TH. Dextran Sulfate Nanocarriers: Design, Strategies and Biomedical Applications. Int J Mol Sci. 2022;24(1).
40. Mi P. Stimuli-responsive nanocarriers for drug delivery, tumor imaging, therapy and theranostics. Theranostics. 2020;10(10):4557-88.
41. Mura S, Nicolas J, Couvreur P. Stimuli-responsive nanocarriers for drug delivery. Nat Mater. 2013;12(11):991-1003.
42. Das SS, Bharadwaj P, Bilal M, Barani M, Rahdar A, Taboada P, et al. Stimuli-Responsive Polymeric Nanocarriers for Drug Delivery, Imaging, and Theragnosis. Polymers (Basel). 2020;12(6).
43. Sun C, Liang Y, Hao N, Xu L, Cheng F, Su T, et al. A ROS-responsive polymeric micelle with a pi-conjugated thioketal moiety for enhanced drug loading and efficient drug delivery. Org Biomol Chem. 2017;15(43):9176-85.
44. Tao W, He Z. ROS-responsive drug delivery systems for biomedical applications. Asian J Pharm Sci. 2018;13(2):101-12.
45. Ruiz-Pulido G, Medina DI, Barani M, Rahdar A, Sargazi G, Baino F, et al. Nanomaterials for the Diagnosis and Treatment of Head and Neck Cancers: A Review. Materials (Basel). 2021;14(13).
46. Zhao W, Feng H, Sun W, Liu K, Lu JJ, Chen X. Tert-butyl hydroperoxide (t-BHP) induced apoptosis and necroptosis in endothelial cells: Roles of NOX4 and mitochondrion. Redox Biol. 2017;11:524-34.
47. Brozek-Pluska B, Beton K. Oxidative stress induced by tBHP in human normal colon cells by label free Raman spectroscopy and imaging. The protective role of natural antioxidants in the form of beta-carotene. RSC Adv. 2021;11(27):16419-34.
48. Gaucher C, Boudier A, Bonetti J, Clarot I, Leroy P, Parent M. Glutathione: Antioxidant

Properties Dedicated to Nanotechnologies. Antioxidants (Basel). 2018;7(5).
49. Tomin T, Schittmayer M, Birner-Gruenberger R. Addressing Glutathione Redox Status in Clinical Samples by Two-Step Alkylation with N-ethylmaleimide Isotopologues. Metabolites. 2020;10(2).
50. Kizek R, Vacek J, Trnkova L, Jelen F. Cyclic voltammetric study of the redox system of glutathione using the disulfide bond reductant tris(2-carboxyethyl)phosphine. Bioelectrochemistry. 2004;63(1-2):19-24.
51. Ucuzian AA, Gassman AA, East AT, Greisler HP. Molecular mediators of angiogenesis. J Burn Care Res. 2010;31(1):158-75.
52. Jiang J, Dong C, Zhai L, Lou J, Jin J, Cheng S, et al. Paeoniflorin Suppresses TBHP-Induced Oxidative Stress and Apoptosis in Human Umbilical Vein Endothelial Cells via the Nrf2/HO-1 Signaling Pathway and Improves Skin Flap Survival. Front Pharmacol. 2021;12:735530.
53. Zhu L, Zang J, Liu B, Yu G, Hao L, Liu L, et al. Oxidative stress-induced RAC autophagy can improve the HUVEC functions by releasing exosomes. J Cell Physiol. 2020;235(10):7392-409.
54. Lopez-Garcia J, Lehocky M, Humpolicek P, Saha P. HaCaT Keratinocytes Response on Antimicrobial Atelocollagen Substrates: Extent of Cytotoxicity, Cell Viability and Proliferation. J Funct Biomater. 2014;5(2):43-57.
55. de Souza GL, Silva ACA, Dantas NO, Turrioni APS, Moura CCG. Cytotoxicity and Effects of a New Cacium Hydroxide Nanoparticle Material on Production of Reactive Oxygen Species by LPS-Stimulated Dental Pulp Cells. Iran Endod J. 2020;15(4):227-35.
56. Nitti M, Marengo B, Furfaro AL, Pronzato MA, Marinari UM, Domenicotti C, et al. Hormesis and Oxidative Distress: Pathophysiology of Reactive Oxygen Species and the Open Question of Antioxidant Modulation and Supplementation. Antioxidants (Basel). 2022;11(8).
57. Brieger K, Schiavone S, Miller FJ, Jr., Krause KH. Reactive oxygen species: from health to disease. Swiss Med Wkly. 2012;142:w13659.
58. Frisard MI, Broussard A, Davies SS, Roberts LJ, 2nd, Rood J, de Jonge L, et al. Aging, resting metabolic rate, and oxidative damage: results from the Louisiana Healthy Aging Study. J Gerontol A Biol Sci Med Sci. 2007;62(7):752-9.
59. Lin J, Shi Y, Miao J, Wu Y, Lin H, Wu J, et al. Gastrodin Alleviates Oxidative Stress-Induced Apoptosis and Cellular Dysfunction in Human Umbilical Vein Endothelial Cells via the Nuclear Factor-Erythroid 2-Related Factor 2/Heme Oxygenase-1 Pathway and Accelerates Wound Healing In Vivo. Front Pharmacol. 2019;10:1273.
60. Villalpando-Rodriguez GE, Gibson SB. Reactive Oxygen Species (ROS) Regulates Different Types of Cell Death by Acting as a Rheostat. Oxid Med Cell Longev. 2021;2021:9912436.
61. Green DR, Galluzzi L, Kroemer G. Cell biology. Metabolic control of cell death. Science. 2014;345(6203):1250256.
62. Zhou D, Shao L, Spitz DR. Reactive oxygen species in normal and tumor stem cells. Adv Cancer Res. 2014;122:1-67.
63. Konno T, Melo EP, Chambers JE, Avezov E. Intracellular Sources of ROS/H(2)O(2) in Health and Neurodegeneration: Spotlight on Endoplasmic Reticulum. Cells. 2021;10(2).
64. Di Meo S, Reed TT, Venditti P, Victor VM. Role of ROS and RNS Sources in Physiological and Pathological Conditions. Oxid Med Cell Longev. 2016;2016:1245049.
65. Liu S, Yang W, Li Y, Sun C. Fetal bovine serum, an important factor affecting the reproducibility of cell experiments. Sci Rep. 2023;13(1):1942.
66. Lee DY, Lee SY, Yun SH, Jeong JW, Kim JH, Kim HW, et al. Review of the Current Research on Fetal Bovine Serum and the Development of Cultured Meat. Food Sci Anim Resour. 2022;42(5):775-99.
67. Feng XJ, Van Hove CE, Walter PJ, Herman AG. Effects of storage temperature and fetal calf serum on the endothelium of porcine aortic valves. J Thorac Cardiovasc Surg. 1996;111(1):218-30.
68. Kwon DH, Cha HJ, Lee H, Hong SH, Park C, Park SH, et al. Protective Effect of Glutathione against Oxidative Stress-induced Cytotoxicity in RAW 264.7 Macrophages through Activating the Nuclear Factor Erythroid 2-Related Factor-2/Heme Oxygenase-1 Pathway. Antioxidants (Basel). 2019;8(4).
69. Musaogullari A, Mandato A, Chai YC. Role of Glutathione Depletion and Reactive Oxygen Species Generation on Caspase-3 Activation: A Study With the Kinase Inhibitor Staurosporine. Front Physiol. 2020;11:998.

70. Irihimovitch V, Shapira M. Glutathione redox potential modulated by reactive oxygen species regulates translation of Rubisco large subunit in the chloroplast. J Biol Chem. 2000;275(21):16289-95.
71. Armstrong JS, Steinauer KK, Hornung B, Irish JM, Lecane P, Birrell GW, et al. Role of glutathione depletion and reactive oxygen species generation in apoptotic signaling in a human B lymphoma cell line. Cell Death Differ. 2002;9(3):252-63.
72. Unterluggauer H, Hampel B, Zwerschke W, Jansen-Durr P. Senescence-associated cell death of human endothelial cells: the role of oxidative stress. Exp Gerontol. 2003;38(10):1149-60.
73. Couto N, Wood J, Barber J. The role of glutathione reductase and related enzymes on cellular redox homoeostasis network. Free Radic Biol Med. 2016;95:27-42.
74. Carlberg I, Mannervik B. Glutathione reductase. Methods Enzymol. 1985;113:484-90.
75. Vaskova J, Kocan L, Vasko L, Perjesi P. Glutathione-Related Enzymes and Proteins: A Review. Molecules. 2023;28(3).
76. Bains VK, Bains R. The antioxidant master glutathione and periodontal health. Dent Res J (Isfahan). 2015;12(5):389-405.
77. Alves AF, Moura AC, Andreolla HF, Veiga A, Fiegenbaum M, Giovenardi M, et al. Gene expression evaluation of antioxidant enzymes in patients with hepatocellular carcinoma: RT-qPCR and bioinformatic analyses. Genet Mol Biol. 2021;44(2):e20190373.
78. Tavleeva MM, Belykh ES, Rybak AV, Rasova EE, Chernykh AA, Ismailov ZB, et al. Effects of Antioxidant Gene Overexpression on Stress Resistance and Malignization In Vitro and In Vivo: A Review. Antioxidants (Basel). 2022;11(12).
79. Paganin M, Tebaldi T, Lauria F, Viero G. Visualizing gene expression changes in time, space, and single cells with expressyouRcell. iScience. 2023;26(6):106853.
80. Wieczorek E, Jablonowski Z, Tomasik B, Gromadzinska J, Jablonska E, Konecki T, et al. Different Gene Expression and Activity Pattern of Antioxidant Enzymes in Bladder Cancer. Anticancer Res. 2017;37(2):841-8.
81. Nandi A, Yan LJ, Jana CK, Das N. Role of Catalase in Oxidative Stress- and Age-Associated Degenerative Diseases. Oxid Med Cell Longev. 2019;2019:9613090.
82. Gupta S, Choi A, Yu HY, Czerniak SM, Holick EA, Paolella LJ, et al. Fluctuations in total antioxidant capacity, catalase activity and hydrogen peroxide levels of follicular fluid during bovine folliculogenesis. Reprod Fertil Dev. 2011;23(5):673-80.
83. Bodega G, Alique M, Bohorquez L, Ciordia S, Mena MC, Ramirez MR. The Antioxidant Machinery of Young and Senescent Human Umbilical Vein Endothelial Cells and Their Microvesicles. Oxid Med Cell Longev. 2017;2017:7094781.
84. Voigt J, Christensen J, Shastri VP. Differential uptake of nanoparticles by endothelial cells through polyelectrolytes with affinity for caveolae. Proc Natl Acad Sci U S A. 2014;111(8):2942-7.
85. Petrovici AR, Pinteala M, Simionescu N. Dextran Formulations as Effective Delivery Systems of Therapeutic Agents. Molecules. 2023;28(3).
86. Carme Coll Ferrer M, Sobolewski P, Composto RJ, Eckmann DM. Cellular Uptake and Intracellular Cargo Release From Dextran Based Nanogel Drug Carriers. J Nanotechnol Eng Med. 2013;4(1):110021-8.
87. Sousa de Almeida M, Susnik E, Drasler B, Taladriz-Blanco P, Petri-Fink A, Rothen-Rutishauser B. Understanding nanoparticle endocytosis to improve targeting strategies in nanomedicine. Chem Soc Rev. 2021;50(9):5397-434.
88. Rasel MAI, Singh S, Nguyen TD, Afara IO, Gu Y. Impact of Nanoparticle Uptake on the Biophysical Properties of Cell for Biomedical Engineering Applications. Sci Rep. 2019;9(1):5859.
89. Duan J, Yu Y, Li Y, Yu Y, Li Y, Zhou X, et al. Toxic effect of silica nanoparticles on endothelial cells through DNA damage response via Chk1-dependent G2/M checkpoint. PLoS One. 2013;8(4):e62087.
90. Shi J, Sun X, Lin Y, Zou X, Li Z, Liao Y, et al. Endothelial cell injury and dysfunction induced by silver nanoparticles through oxidative stress via IKK/NF-kappaB pathways. Biomaterials. 2014;35(24):6657-66.
91. Soenen SJ, De Backer L, Manshian B, Doak S, Raemdonck K, Demeester J, et al.

Unraveling the effects of siRNA carrier systems on cell physiology: a multiparametric approach demonstrated on dextran nanogels. Nanomedicine (Lond). 2014;9(1):61-76.
92. Wen T, Yang A, Piao L, Hao S, Du L, Meng J, et al. Comparative study of in vitro effects of different nanoparticles at non-cytotoxic concentration on the adherens junction of human vascular endothelial cells. Int J Nanomedicine. 2019;14:4475-89.
93. Pamela Ubaldo HA, Franklin Cavender ,Jay Means ,Dale Hales ,Lichang Wang Osmotic pressure induced toxicity by aggregation of citrate-coated silver nanoparticles inside HepG2 cells. ChemRxiv 29 November 2022.
94. Rizwan H, Pal S, Sabnam S, Pal A. High glucose augments ROS generation regulates mitochondrial dysfunction and apoptosis via stress signalling cascades in keratinocytes. Life Sci. 2020;241:117148.
95. Ph.D. HE-OMDMLC. Mitochondrial ROS and Apoptosis. 14 September 2016.
96. Ghanian Z, Konduri GG, Audi SH, Camara AKS, Ranji M. Quantitative optical measurement of mitochondrial superoxide dynamics in pulmonary artery endothelial cells. J Innov Opt Health Sci. 2018;11(1).
97. Kalinovic S, Oelze M, Kroller-Schon S, Steven S, Vujacic-Mirski K, Kvandova M, et al. Comparison of Mitochondrial Superoxide Detection Ex Vivo/In Vivo by mitoSOX HPLC Method with Classical Assays in Three Different Animal Models of Oxidative Stress. Antioxidants (Basel). 2019;8(11).
98. Milkovic L, Cipak Gasparovic A, Cindric M, Mouthuy PA, Zarkovic N. Short Overview of ROS as Cell Function Regulators and Their Implications in Therapy Concepts. Cells. 2019;8(8).
99. Soragni C, Rabussier G, Lanz HL, Bircsak KM, de Windt LJ, Trietsch SJ, et al. A versatile multiplexed assay to quantify intracellular ROS and cell viability in 3D on-a-chip models. Redox Biol. 2022;57:102488.
100. Merck KGaA D, Germany and/or its affiliates. DCFHDA Merck2024 [
101. Duan J, Du J, Jin R, Zhu W, Liu L, Yang L, et al. Iron oxide nanoparticles promote vascular endothelial cells survival from oxidative stress by enhancement of autophagy. Regen Biomater. 2019;6(4):221-9.
102. Ott M, Robertson JD, Gogvadze V, Zhivotovsky B, Orrenius S. Cytochrome c release from mitochondria proceeds by a two-step process. Proc Natl Acad Sci U S A. 2002;99(3):1259-63.
103. Liu X, Gao RW, Li M, Si CF, He YP, Wang M, et al. The ROS derived mitochondrial respirstion not from NADPH oxidase plays key role in Celastrol against angiotensin II-mediated HepG2 cell proliferation. Apoptosis. 2016;21(11):1315-26.
104. Rasmussen MK, Pedersen JN, Marie R. Size and surface charge characterization of nanoparticles with a salt gradient. Nat Commun. 2020;11(1):2337.
105. Clogston JD, Patri AK. Zeta potential measurement. Methods Mol Biol. 2011;697:63-70.
106. Jeon S, Clavadetscher J, Lee DK, Chankeshwara SV, Bradley M, Cho WS. Surface Charge-Dependent Cellular Uptake of Polystyrene Nanoparticles. Nanomaterials (Basel). 2018;8(12).
107. Rinaldi A, Caraffi R, Grazioli MV, Oddone N, Giardino L, Tosi G, et al. Applications of the ROS-Responsive Thioketal Linker for the Production of Smart Nanomedicines. Polymers (Basel). 2022;14(4).
108. Mascone SE, Kim KI, Evans WS, Prior SJ, Cook MD, Ranadive SM. Race and sex differences in ROS production and SOD activity in HUVECs. PLoS One. 2023;18(10):e0292112.
109. Lee D, Bae S, Hong D, Lim H, Yoon JH, Hwang O, et al. H2O2-responsive molecularly engineered polymer nanoparticles as ischemia/reperfusion-targeted nanotherapeutic agents. Sci Rep. 2013;3:2233.
110. Ye X, Gaucher JF, Vidal M, Broussy S. A Structural Overview of Vascular Endothelial Growth Factors Pharmacological Ligands: From Macromolecules to Designed Peptidomimetics. Molecules. 2021;26(22).
111. Barzkar N, Babich O, Das R, Sukhikh S, Tamadoni Jahromi S, Sohail M. Marine Bacterial Dextranases: Fundamentals and Applications. Molecules. 2022;27(17).
112. Xu Y, Wang H, Lin Q, Miao Q, Liu M, Ni H, et al. Immobilization of Dextranase Obtained from the Marine Cellulosimicrobium sp. Y1 on Nanoparticles: Nano-TiO(2) Improving Hydrolysate Properties and Enhancing Reuse. Nanomaterials (Basel). 2023;13(6).
113. Semyonov D, Ramon O, Shoham Y, Shimoni E. Enzymatically synthesized dextran

nanoparticles and their use as carriers for nutraceuticals. Food Funct. 2014;5(10):2463-74.
114. Ritz U, Eberhardt M, Klein A, Frank P, Gotz H, Hofmann A, et al. Photocrosslinked Dextran-Based Hydrogels as Carrier System for the Cells and Cytokines Induce Bone Regeneration in Critical Size Defects in Mice. Gels. 2018;4(3).
115. Guzman-Hernandez ML, Potter G, Egervari K, Kiss JZ, Balla T. Secretion of VEGF-165 has unique characteristics, including shedding from the plasma membrane. Mol Biol Cell. 2014;25(7):1061-72.
116. Akbarian M, Chen SH. Instability Challenges and Stabilization Strategies of Pharmaceutical Proteins. Pharmaceutics. 2022;14(11).
117. Chen SY, Zacharias M. What Makes a Good Protein-Protein Interaction Stabilizer: Analysis and Application of the Dual-Binding Mechanism. ACS Cent Sci. 2023;9(5):969-79.
118. Pas T, Struyf A, Vergauwen B, Van den Mooter G. Ability of gelatin and BSA to stabilize the supersaturated state of poorly soluble drugs. Eur J Pharm Biopharm. 2018;131:211-23.
119. Chang BS, Mahoney RR. Enzyme thermostabilization by bovine serum albumin and other proteins: evidence for hydrophobic interactions. Biotechnol Appl Biochem. 1995;22(2):203-14.
120. Stone D, Phaneuf M, Sivamurthy N, LoGerfo FW, Quist WC. A biologically active VEGF construct in vitro: implications for bioengineering-improved prosthetic vascular grafts. J Biomed Mater Res. 2002;59(1):160-5.

Acknowledgements – Acknowledgements – The authors extend their sincere thanks to Prof. Dr. Ethirajan A. and Nayak S. (Institute for Materials Research (IMO-IMOMEC) at Hasselt University, Diepenbeek, Belgium) for providing the ROS-sensitive dextran NCs and the samples to perform the ELISA for the VEGF release study. Additionally, heartfelt gratitude is expressed to the fellow students and PhD students of the research group. Special thanks are also extended to Pirlet E for her invaluable guidance and assistance throughout the experiments and Bronckaers A. for her knowledge and insights.

Author contributions – Bronckaers A. and Pirlet E. conceived and designed the research. Pirlet E. and Eerdekens H. conducted the experiments. Eerdekens H. performed data analysis and drafted the manuscript. Pirlet E. meticulously revised and edited the manuscript. All authors have approved the final version of the manuscript.

SUPPLEMENTARY TABLES

Table S1 – Human primer sets for qPCR analysis.

Gene	*Primer*	*Sequence (5'-3')*
SOD 1	*Forward*	CTCACTCTCAGGAGACCATTGC
	Reverse	CCACAAGCCAAACGACTTCCAG
SOD 2	*Forward*	TTTCAATAAGGAACGGGGACAC
	Reverse	GTGCTCCCACACATCAATCC
CAT	*Forward*	TGGGATCTCGTTGGAAATAACAC
	Reverse	TCAGGACGTAGGCTCCAGAAG
GpX 1	*Forward*	GTGCTCGGCTTCCCGTGCAAC
	Reverse	CTCGAAGAGCATGAAGTTGGGC
GpX4	*Forward*	ACAAGAACGGCTGCGTGGTGAA
	Reverse	GCCACACACTTGTGGAGCTAGA
Gr	*Forward*	TTCCAGAATACCAACGTCAAAGG
	Reverse	GTTTTCGGCCAGCAGCTATTG
NRF2	*Forward*	CACATCCAGTCAGAAACCAGTGG
	Reverse	GGAATGTCTGCGCCAAAAGCTG
NQO1	*Forward*	GAAGAGCACTGATCGTACTGGC
	Reverse	GGATACTGAAAGTTCGCAGGG

SOD1, superoxide dismutase 1; SOD2, superoxide dismutase 2; CAT, catalase; gpX1, glutathione peroxidase; pgX4, glutathione peroxidase; Gr, glutathione reductase; NRF2, nuclear factor erythroid 2-related factor 2, NQO1, NAD(P)H quinone oxidoreductase.

SUPPLEMENTARY FIGURES

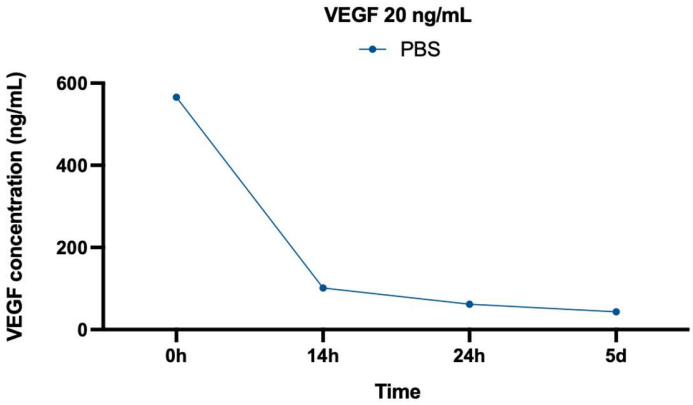

Figure S1: VEGF stability decreases over time. *ELISA detecting VEGF concentration after incubating 20ng/mL VEGF with PBS for 0h, 14h, 24h, and 5 days. V*EGF levels strongly decline from 0h to 14h and then decrease slightly up to 5 days.

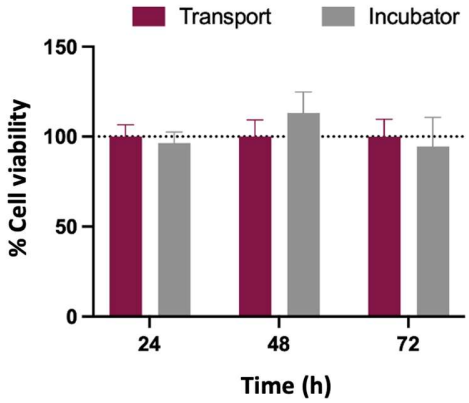

Figure S2: The transport process did not impact HUVEC cell viability. *Alamar Blue cell viability assay of* HUVECs incubated in the cell culture incubator and HUVECs transported to the x-ray irradiator. Data shows no difference in viability between the two, indicating no effect of transportation on cell viability. *Data is normalized to the untreated control (dotted line). n=2. All data are represented as mean ± SEM.*

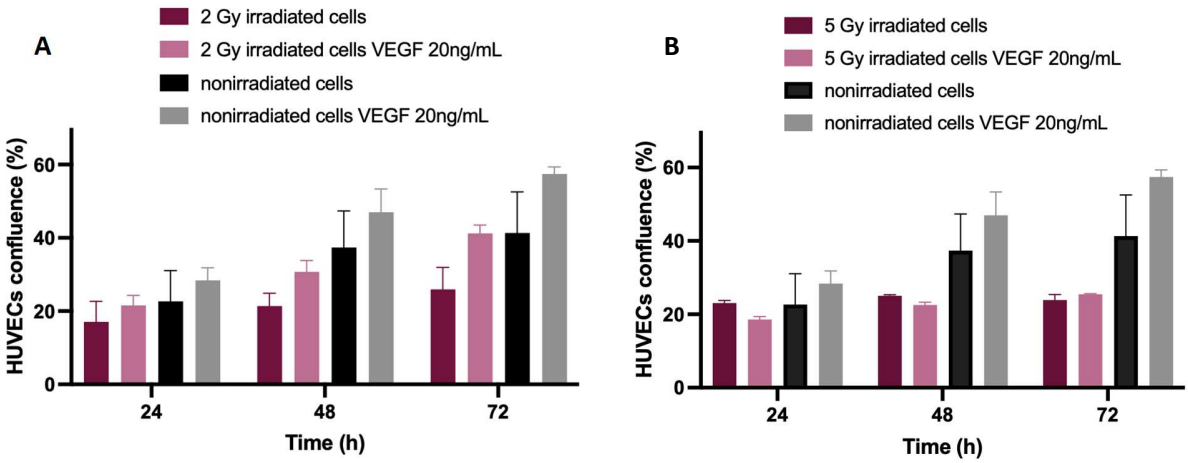

Figure S3: 2 Gy and 5 Gy X-ray irradiation negatively impact VEGF stability. *HUVECs confluence was measured using a proliferation assay after exposure to low energy X-ray irradiation at 2 Gy* ***(A)*** *and 5 Gy* ***(B)*** *and subsequent treatment with 20 ng/ml of VEGF for 72h. Data shows that VEGF continues to promote cell proliferation after irradiation with 2 and 5 Gy, albeit at a reduced level compared to nonirradiated negative control cells. n=1. All data are represented as mean ± SEM.*